Scholars' Mine

Masters Theses   Student Theses and Dissertations

Spring 2012

Cerium-based conversion coatings on cast aluminum 380 and 413 alloys

Ci Lin

Recommended Citation

Lin, Ci, "Cerium-based conversion coatings on cast aluminum 380 and 413 alloys" (2012). *Masters Theses*. 4147.
https://scholarsmine.mst.edu/masters_theses/4147

CERIUM-BASED CONVERSION COATINGS

ON CAST ALUMINUM 380 AND 413 ALLOYS

by

CI LIN

A THESIS

Presented to the Faculty of the Graduate School of the

MISSOURI UNIVERSITY OF SCIENCE AND TECHNOLOGY

In Partial Fulfillment of the Requirements for the Degree

MASTER OF SCIENCE

IN

MATERIALS SCIENCE AND ENGINEERING

2012

Approved by

W. Fahrenholtz, Advisor
M.J. O'Keefe, Co-Advisor
S. Maddela

PUBLICATION THESIS OPTION

This thesis has been prepared in the style utilized by Corrosion Science and the Journal of the Electrochemical Society. It consists of two papers be submitted for publication. The first paper (pages 18-41) is intended for submission to Corrosion Science. The second paper (pages 42-69) is intended for future publication in the Journal of the Electrochemical Society.

ABSTRACT

This investigation focused on the deposition and characterization of cerium-based conversion coatings (CeCCs) on cast aluminum alloys. Previous research has shown that CeCCs are viable alternatives to chromate conversion on high strength alloys such as 2024-T3 and 7075-T6. For the casting alloys such as 380 and 413, the presence of Si affects the composition and stability of the native oxide, which means that pretreatment plays an important role for the coating deposition. This thesis consists of two papers that describe the results of the study.

The first paper reports the effect of the final rinsing temperature before coating deposition on coating morphology, thickness, and corrosion performance. The AA 380 panels were activated in 60°C sulfuric acid and rinsed at 25°C or 100°C in distilled water before immersion in the coating solution for 2, 5, and 8 minutes. The morphology and thickness data suggest that rinsing at 25°C resulted in a faster deposition rate, but less corrosion resistance due to cracking. However, rinsing at 100°C reduced the deposition rate, but increased corrosion resistance by producing a more homogeneous coating.

The second paper focused a deposition of cerium-based conversion coatings on aluminum 413 and 380 alloys under the assistance of ultrasound. Electrochemical impedance spectroscopy and the potentiodynamic measurements showed that ultrasound increased impedance and reduced the corrosion current. The morphology of coatings deposited with ultrasound showed reduced cracking. The salt spray corrosion testing (ASTM B117) showed that CeCCs deposited with ultrasound wave had better corrosion resistance than coatings deposited using the conventional process.

ACKNOWLEDGMENTS

TABLE OF CONTENT

SECTION

LIST OF ILLUSTRATIONS

Figure   Page

LIST OF TABLES

1. INTRODUCTION

1.1. HISTORY OF CERIUM CONVERSION COATING

Cerium-based conversion coatings (CeCCs) have been proposed as an environmentally friendly alternative to chromate-based conversion coatings (CrCCs) for corrosion protection of high strength aluminum alloys [1-15]. Numerous studies have shown that CrCCs are highly effective coatings for corrosion protection of a variety of metals [16-21]. However, hexavalent chromium has been identified as a carcinogen; thus, there is considerable effort in finding an alternative to CrCCs. The pioneering research conducted by Hinton et al. [7-10] has shown that CeCCs deposited on high strength aluminum alloys were capable of providing significant corrosion protection. Since then many groups have investigated CeCCs for corrosion protection of metals [1-6, 14-21]. This research focused on deposition, morphology, and the corrosion protection mechanism of CeCCs on casting aluminum 380 and 413 alloys.

1.2. RESEARCH OBJECTIVE

The initial research objective was to develop a new method for deposition of corrosion resistant CeCCs on Al 380 and 413 alloys. In order to obtain good coatings, attention was paid to the mechanism of coating deposition as well as the thermodynamic and kinetic aspects of the coating deposition. It found that coating deposition was affected by the panel temperature. So, this research concentrated on the temperature of the panel before the coating. Additional research examined the structure of CeCCs that was modified by applying ultrasound during deposition. The scientific contributions of this research are described in two manuscripts that make up the body of the thesis.

Paper I. The first paper described the effect of final water rinsing temperature prior to the immersion on the chemical composition and thickness the surface oxide layer on Al 380 alloy. The paper develops a method using different rinsing temperatures, one at 25°C and another at 100°C, followed by immersion in the coating solution for 2, 5, or 8 minutes. The main outcome of the paper was identification of the 100°C rinse as a promising approach to deposit coatings with improved corrosion resistance.

Paper II. The second paper reported the effect of ultrasound on the coating morphology and thickness as well as the morphology of the interface between the substrate and coating on aluminum 413 and 380 alloys. Coatings deposited under the assistance of ultrasound performed differently due to differences in morphology and thickness, which would lead to improved corrosion resistance.

2. LITERATURE REVIEW

2.1. CASTING ALUMINUM ALLOY

Aluminum (Al) is a soft, durable, silvery-white lightweight metal with a density of 2.70 g/cm^3 which is about one-third the density of steel. Pure annealed aluminum (99.99%) has a tensile strength of 45 MPa, yield strength of 10 MPa, and is very corrosion resistant [22, 23, 24]. However, in order to change the properties of the aluminum, other elements such as copper, silcon or zinc are added to improve its mechanical properties and refine its grain size [25]. Because of the existance of the second phases, which lead to the pitting corrosion, chromate conversion coatings have been wildly used to protect the alloy from the corrosion [26-29].

Al–Si alloys constitute 80% of the aluminium casting alloys due to their high fluidity, high resistance to corrosion, good weldeability, reduction in shrinkage and low coefficient of thermal expansion, etc. [30]. Eutectic alloys with a high degree of fluidity and low shrinkage on solidification are mainly used for the applications where strength is not a criterion such as domestic cookware, pump castings, manifolds, etc. When as-cast alloys are subjected to elevated temperature they tend to experience growth due to the precipitation of silicon from solid solution. Strengthening of Al–Si alloys is possible by the addition of other alloying elements like Cu and Mg.

2.2. CORROSION OF ALUMINUM ALLOYS

When aluminum surfaces are exposed to the atmosphere, a thin oxide skin forms immediately, this protects the metal from further oxidation. This self-protecting characteristic gives nominally pure aluminum its high resistance to corrosion. Unless exposed to some substance or condition, such as acid [31] or biological organisms [32] or

low pH values [33], which destroys this protective oxide coating, the metal remains fully protected against corrosion. Aluminum alloys can suffer different kinds of corrosion, such as: pitting corrosion, crevice corrosion, poultice corrosion, intergranular and exfoliation corrosion, etc. [34]. Pitting corrosion is the most common phenomenon and widely studied by the laboratory [35-38]. Other types of corrosion can be mitigated or eliminated by proper design, proper fabrication, or the choice of appropriate materials; however, pitting corrosion occurs in halide-containing environments such as near salt water that cannot be changed and are therefore difficult to control. Thus, this research focused on mitigation of pitting corrosion on cast aluminum 380 and 413 alloys by cerium-based conversion coatings (CeCCs).

2.3. ELECTROCHIMAL TESTING

The classical electrochemical methods are based on the simultaneous measurement of current and electrode potential. In simple cases the measured current is proportional to the rate of an electrochemical reaction. However, generally the concentrations of the reacting species at interfaces are different from those in the bulk, since they are depleted or accumulated during the course of the reaction. Here, several electrochemical tests are used to study the corrosion and anti-corrosion behavior of bare substrates and coated specimens.

Simon Joshi et al. [39] have used electrochemical testing to characterize the surface oxide after the alkaline treatments on aluminum alloy 7075-T6. They demonstrated that pitting corrosion was more severe when using a test electrolyte at pH of 5.5 than at pH of 9.0. The electrochemical impedance spectroscopy (EIS) data were fit to an equivalent circuit with two time constants, which represented the properties of a

bulk oxide and the corrosion pits. The reduction in overall resistance after pretreatment indicated that the native oxide layer was more susceptible to corrosion, which, in turn, made it easier for the conversion coating solution to penetrate the oxide and react with the substrate to form spontaneous coatings.

In order to characterize the intermetallic phases in the aluminum alloy, Birbilis, and Buchheit [40] developed as electrochemical experiment to test the E_{corr} and i_{corr} of second phases; such as Al_3Fe, Al_2Cu, Al_6Mn, etc. In the present research, a similar electrochemical test was used for obtain the corrosion current, corrosion potential, pitting potential and impedance of panels and coatings. From analysis of these data, the properties of the CeCCs deposited by different methods were studied.

2.4. CERIUM-BASED CONVERSION COATINGS

Pioneering research by Hinton et al. found that CeCCs are an environmentally benign alternative to CrCCs for the protection of aluminum alloys against pitting corrosion [7-10,41]. Their research showed that the maximum corrosion resistance was achieved by long-term exposure (200 hours) under open circuit potential (OCP) conditions to the conversion coating solution. This treatment resulted in an almost complete replacement of the natural aluminum oxide by a protective and durable cerium oxide/hydroxide film. Polarization experiments suggested that the conversion coatings were deposited at cathodic sites such as copper-rich IMCs, thereby suppressing the oxygen reduction reaction that occurred during the corrosion process [8,42]. This suppression in turn led to reduced values of i_{corr} and significant separations between E_{pit} and E_{corr} Thus, CeCCs were identified as cathodic inhibitors during the corrosion process that lead to improved corrosion resistance.

CeCCs can be deposited using both spontaneous and non-spontaneous methods [46]. In both cases, the protective cerium oxide/hydroxide coating forms by a precipitation mechanism that depends on electrochemical potential, pH, dissolved oxygen, and the presence of hydrogen peroxide in the solution. In the original research conducted by Hinton et al. [7-10,41,43], it took about 200 hours to deposit a coating that was about 100 nm thick. The deposition solution used by Hinton did not contain hydrogen peroxide or any other oxidizing compound. The local pH increase resulting from the reduction of dissolved oxygen at cathodic sites by the reaction expressed in equation (1) permits precipitation of Ce(OH)$_3$ and/or Ce(OH)$_4$. The Ce(III) is then oxidized to Ce(IV) by reactions such as the one shown as Reaction (2) [43,44]:

$$O_2(aq) + 2H_2O_2 + 4e^- \rightarrow 4OH^-(aq) \tag{1}$$

$$4Ce^{3+}(aq) + O_2(aq) + 4OH^-(aq) + 2H_2O \rightarrow 4Ce(OH)_2^{2+}(aq) \tag{2}$$
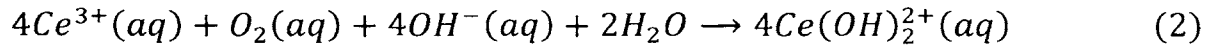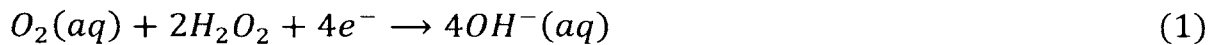
When hydrogen peroxide (or another oxidizer) is added to CeCC deposition solutions, the peroxide is reduced at cathodic sites as indicated by equation (1). For example, previous research used a 1:3 molar ratio of CeCl$_3$ to H$_2$O$_2$ [45]. The OH$^-$ ions generated by this reaction increased the pH of the solution above the solubility limit of cerium species, thereby promoting precipitation of species such as CeO$_2$•2H$_2$O or Ce(OH)$_4$ on the alloy surface. Hydrogen peroxide also acts as an oxidant by oxidizing Ce(III) to Ce(IV) in solution. The reactions for precipitation and coating formation in the presence of peroxide are thought to be as follows [43,44]:

$$Ce^{3+}(aq) + 3OH^- \rightarrow Ce(OH)_3(s) \tag{3}$$

$$Ce^{3+}(aq) + OH^-(aq) + \frac{1}{2}H_2O_2 \longrightarrow Ce(OH)_2^{2+}(aq) \tag{4}$$
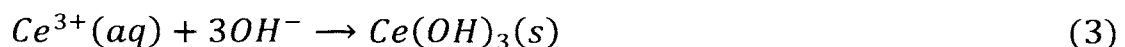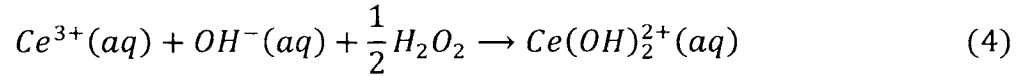
The soluble cerium species such as $Ce(OH)_2^{2+}$ precipitate as insoluble hydroxides, hydrated oxides, and/or peroxy-containing species (Reaction 5) due to the local pH increase near the alloy surface, which is caused by reduction of water and/or the production of OH^- ions by processes such as those describes in Reaction (1):

$$Ce(OH)_2^{2+}(aq) + 2OH^-(aq) \longrightarrow 4Ce(OH)_4(s) \longrightarrow CeO_2 \bullet 2H_2O(s) \tag{5}$$

Post-treatment in heated phosphate solutions ($\geq$ 85°C) enhances the corrosion resistance of CeCCs. During phosphate post-treatment, precipitated species such as $Ce(OH)_4$ and $CeO_2 \bullet 2H_2O$ are converted to $CePO_4 \bullet H_2O$. Coatings that undergo post-treatment have fewer or smaller cracks than as-deposited coatings [46,47]. Post-treated coatings also perform much better in salt spray testing per ASTM B117 than as-deposited coatings [46]. Electrochemical tests have shown improvements in corrosion resistance by a reduction of i_{corr}, an increase in E_{corr} and E_{pit}, and an increase in total impedance [46,47].

2.5. APPLICATION OF ULTRASOIC ENERGY

Ultrasound is a tool to with many different uses. For example, ultrasound is used in the field of cardiovascular diagnosis [48,49], metal defect detection [50,51], corrosion characterization [52-56] and chemical analysis [57-59]. In these and other applications, ultrasound-based techniques are accepted as effective methods for applications in which other method are not effective in obtaining the desired results.

For corrosion, ultrasound is known for its dual effect on the formation and breakdown of passivity on metal surfaces [56]. As an interfacial process, corrosion is related to three parameters mass transport, surface state, and temperature, each of which can be dramatically changed under the irritation of ultrasound.

A number of recent studies have been undertaken concerning the influence of ultrasound on electrodeposition. The influence of ultrasonic energy with a frequency of 20 kHz has been studied on the mechanism of deposition of zinc, lead, cobalt and mercury on glassy carbon [60]. Using cyclic voltammetry, the authors concluded that in electrodeposition or plating under ultrasonic irritation enhanced mass transport enough to change the deposition mechanisms from diffusion-controlled to charge transfer controlled. Ultrasound also affects microstructure as was shown for the electroplating of iridium on copper in aqueous hexabromoiridate(III) solution, where it was observed that fewer defects such as cracks formed using ultrasonication[61].

Zheng et al. also investigated the morphology, electrochemical properties and Vickers hardness of the nanocomposite coatings of Zn-Ni-Al$_2$O$_3$, which were fabricated by electrodeposition[62]. The authors found all of the tested parameters improved significantly, and the corrosion protection was not only related to the dispersion and combination state of nano-alumina particles in the matrix, but also related to the nano-alumina content in the composite coating. Various other studies are concerned with the influence of the power and frequency of ultrasound waves on the deposition rate, nucleation rate, morphology, and electrochemical properties of coatings [63-68].

2.6. ELECTROCHEMICAL IMPEDANCE SPECTROSCOPY

Electrochemical Impedance Spectroscopy (EIS) is a map of the internal distribution of electrical conductivity σ and dielectric permittivity ε in an area of a test specimen. In the process, electrodes are placed in contact with the surface of the region being studied, and the response currents and/or voltages, which are induced by the current or voltage stimuli, are measured at some or all of the electrodes. As a relatively new and powerful method of characterizing many of the electrical properties of materials and their interfaces with electronically conducting electrodes, EIS is broadly used by scientist to investigate the dynamics of bound or mobile charges in the bulk or interfacial regions of many different kinds of physical material or living cell: ionic, semiconducting, mixed electronic-ionic and even insulators (dielectrics) [69-72].
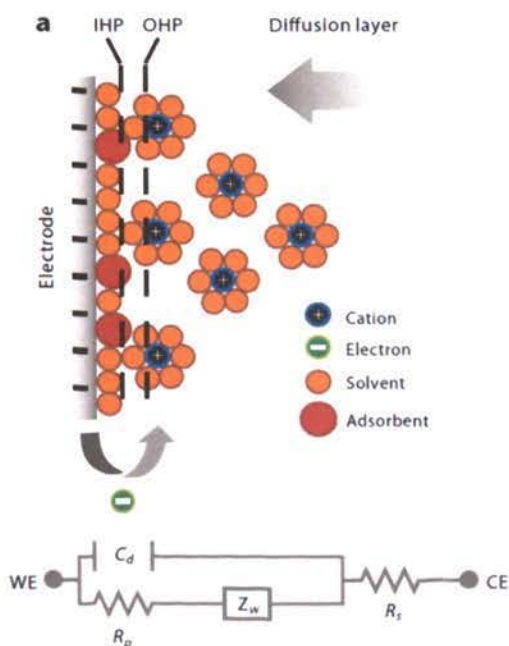
Figure 1. Schematic of an electrified interface in which the electrode is negatively charged and countercations are aligned along the electrified surface. At bottom are the electrical circuit elements corresponding to each interface component. Abbreviations: C_d, double-layer capacitor; CE, counterelectrode; IHP, inner Helmholtz plane; OHP, outer Helmholtz plane; R_p, polarization resistance; R_s, solution resistance; WE, working electrode; Z_W, Warburg impedance. This schematic is from reference 73.

To provide a physical interpretation of EIS data, electrical equivalent circuits (EECs) are used to predict responses similar to those that are measured. Typically, EECs focus on reactions that happen near interfaces. However, EECs are analogs not models, and hence the information that they can deliver on the physico-electrochemical processes that produce the measured responses is limited. As described in a review by Macdonald [74], the utility of EIS arises from four points: (i) it is a linear technique, which means that the results can be interpreted using linear systems theory[75]; (ii) if measured over an infinite frequency range, EIS data contain all of the information that can be gleaned from the system by linear electrical perturbation response techniques; (iii) the experimental efficiency (amount of information transferred to the observer compared to the amount produced by the experiment) is high; and (iv) the validity of the data is readily determined using integral transform techniques, such as the Kramers–Kronig transforms, that are independent of the physical processes involved. Therefore, mathematical interpretation is a key to interpreting EIS data and applying EIS to corrosion problems.

Sunil et al. [76] developed three mathematical models for the proton exchange membrane (PEM) fuel cells based on three different reaction mechanisms. By comparing simulated results with EIS data, they proved that the formation of hydrogen peroxide is an intermediate in a two-step oxygen reduction reaction. As part of the same study, experimental evidence indicated that dissolution of Pt was associated with a decrease in catalytic activity. In a companion paper [77], Sunil et al. also analyzed differences between the impedance response of PEM fuel cell and their EEC. In some cases, the differences were attributed to low-frequency inductance, which was consistent with the

Kramer–Kronig relations, while in other cases nonstationary phenomena were found to have influenced the low-frequency response.

REFERENCES

1. B. Y. Johnson, J. Edington, M. J. O'Keefe, Materials Science & Engineering, A: Structural Materials: Properties, Microstructure and Processing, A361 (1-2), 225 – 231 (2003).

2. W. G. Fahrenholtz, M. J. O'Keefe, H. Zhou, J. T. Grant, Surf. Coat. Tech. 155, 208–213 (2002).

3. S. Geng, P. Yu, M. J. O'Keefe, W. G. Fahrenholtz, and T. J. O'Keefe, J. Applied Electrochemistry, Accepted for publication, (October 2009).

4. W. Pinc, S. Geng, M. O'Keefe, W. Fahrenholtz and T. O'Keefe, Applied Surface Science, 255, 4061–4065 (2009).

5. B. L. Treu, S. Joshi, W. R. Pinc, M. J. O'Keefe, and W. G. Fahrenholtz, ECS.T 19, 101-113 (2009).

6. S. Joshi, M. J. O'Keefe, and W. G. Fahrenholtz, ECS.T 25, 19-30 (2010).

7. B.W.R. Hinton, D.R. Arnott, N.E. Ryan, Mater. Forum, 7 (4) 211-217 (1984).

8. B.W.R. Hinton, D.R. Arnott, and N.E. Ryan, Mater. Forum, 9 (3) 162-173 (1986).

9. B.W.R. Hinton, J. Alloys Compd., 180 15-25 (1992).

10. B.W.R. Hinton, N.E. Ryan, and D.R. Arnott, Mater. Australasia, 19 (1) 18-20 (1987).

11. F. H. Scholes, C. Soste, A. E. Hughes, S. G. Hardin, and P. R. Curtis, Applied Surface Science, 253, 1770-1780, (2006).

12. S. A. Hayes, P. Yu, T. J. O'Keefe, M. J. O'Keefe, and J. O. Stoffer, J. Electrochem. Soc., 149 C623-C630 (2002).

13. B. F. Rivera, B. Y. Johnson, M. J. O'Keefe, and W. G. Fahrenholtz, Surf. Coat. Tech, 173, 349-356, (2004)

14. A.de Frutos, M. A. Arenas, Y. Liu, P. Skeldon, G. E. Thompson, J. de Damborena, A.Conde, Surf. Coat. Tech, 202, 3797-3807, (2008).

15. D. K. Heller, W. G. Fahrenholtz, and M. J. O'Keefe, J. Electrochem. Soc., 156 C400-C406 (2009).

16. P. Campestrini, E.P.M. van Westing, J. H. W. de Wit, Electrochimica Acta, 46, 2553-2571 (2001).

17. S. A. Kulinich, A. S. Akhtar, D. Susac, P. C. Wong, K. C. Wong, K. A. R. Mitchell, Applied Surface Science, 253, 3144-3153 (2007).

18. S. M. Cohen, Corrosion, 51, 71-78 (1995).

19. L. Wilson, B.W.R. Hinton, A Method of Forming a Corrosion Resistant Coating,International Patent WO 88/06639.

20. J. R. Waldrop and M. W. Kendig, J. Electrochem. Soc., 145, L11-13 (1998).

21. J. Zhao, L. Xia, A. Sehgal, D. Lu, R. L. McCreery, and G. S. Frankel, Surface and Coatings Technology, 140, 51-57 (2001).

22. D. R. Askeland, "The Science and Engineering of Materials". Springer, (1984).

23. J. E. Hatch, Aluminum: Properties and Physical Metallurgy, ASM (1984).

24. E. L. Rooy, ASM Handbook, 2, (2002).

25. Mark Easton, Cameron Davidson, and David St John, Effect of Alloy Composition on the Dendrite Arm Spacing of Multicomponent Aluminum Alloys, Volume 41A,2010,1528-1538.

26. Burstein, G T;Liu, C;Souto, R M;Vines, S P,Origins of pitting corrosion, Corrosion Engineering, Science, and Technology; Mar 2004; 39, 1.

27. Illevbare, G O;Scully, J R;Yuan, J;Kelly, R G,Inhibition of pitting corrosion on aluminum alloy 2024-T3: Effect of soluble chromate additions vs Chromate Conversion coating, Corrosion; Mar 2000; 56, 3.

28. Blackwood, D J;Chong, A S L,Pitting corrosion on aluminium in absence of chloride, Corrosion Engineering, Science, and Technology; 1998; 33, 3.

29. Z. Ahmad, Saudi Arabia, P. T. Paulette, B. J. A. Aleem, Mechanism of localized corrosion of aluminum–silicon carbide composites in a chloride containing environment, Journal of Material Science, 35 (2000) 2573 – 2579.

30. Sathyapal Hegde .K. Narayan Prabhu, Modification of eutectic silicon in Al–Si alloys, J Mater Sci (2008) 43:3009–3027.

31. Rosliza Ramli, S. Y. Seoh, W. B. Wan Nik and H. B. Senin, Corrosion Behavior of Aluminum Alloys in Acidic Media, Solid State Science and Technology, ICSSST 2006,220-222.

32. V. F. Smirnov, D. V. Belov, T. N. Sokolova, O. V. Kuzina, and V. R. Kartashov, Microbiological Corrosion of Aluminum Alloys, Applied Biochemistry and Microbiology, 2008, Vol. 44, No. 2, pp. 192–196.

33. B. Zaid , D. Saidi , A. Benzaid , S. Hadji, Effects of pH and chloride concentration on pitting corrosion of AA6061 aluminum alloy, Corrosion Science 50 (2008) 1841–1847.

34. J. Gilbert Kaufman, Elwin L. Rooy, "Aluminum Alloy Castings: Properties, Processes, and Applications," (Materials Park, OH: American Society for Materials International, 2004), pp.45-74.

35. A.P. Boag, D.G. McCulloch, D.N. Jamieson, A.E. Hughes, L.M. Pedrina and C.G. Ryan, Analysis of Pitting Corrosion in Aerospace Aluminium Alloy AA2024-T3, Microscopy and Microanalysis 11. S02 (Aug 2005): 1984-1985.

36. J. M. Bastidas, A. Forn, M. T. Baile, J. L. Polo and C. L. Torres, Pitting corrosion of A357 aluminium alloy obtained by semisolid processing, Materials and Corrosion 52, 691-696 (2001).

37. G.T.Burstein, C. Liu, R.M. Souto and S.P. Vines, Origins of Pitting Corrosion, Corrosion Engineering, Science and Technology, 39 1, 25-30 (2004).

38. G. S Peng, K. H. Chen, H. C. Fang, H. Chao and S. Y. Chen, EIS study on pitting corrosion of 7150 aluminum alloy in sodium chloride and hydrochloric acid solution, Materials and Corrosion 2010, 61 No. 9.

39. Simon Joshi, William G. Fahrenholtz, and Matthew J. O'Keefe, Electrochemical Characterization of Al 7075-T6 Surface Oxide After Alkaline Treatments, Journal of The Electrochemical Society, 158 (9) C296-C301 (2011).

40. N. Birbilis, and R. G. Buchheit, Electrochemical Characteristics of Intermetallic Phases in Aluminum Alloys, Journal of The Electrochemical Society, 152 (4) B140-B151(2005)

41. L. Wilson, B.W.R. Hinton, A Method of Forming a Corrosion Resistant Coating, International Patent WO 88/06639.

42. W. Pinc, S. Maddela, W. Fahrenholtz, and M O'Keefe, Surf. Coat. Technol. 204 (2010) 4095-4100.

43. F. H. Scholes, C. Soste, A. E. Hughes, S. G. Hardin, and P. R. Curtis, Applied Surface Science, 253, 1770-1780, (2006).

44. S. A. Hayes, P. Yu, T. J. O'Keefe, M. J. O'Keefe, and J. O. Stoffer, J. Electrochem. Soc., 149 C623-C630 (2002).

45. W. Pinc, S. Geng, M. O'Keefe, W. Fahrenholtz and T. O'Keefe, Applied Surface Science, 255, 4061–4065 (2009).

46. D. K. Heller, W. G. Fahrenholtz, and M. J. O'Keefe, J. Electrochem. Soc., 156 C400-C406 (2009).

47. H. Zhang and Y. Zuo, Applied surface Science, 254, 4930-4935, (2008).

48. Jonathan R. Lindner, Contrast ultrasound molecular imaging of inflammation in cardiovascular disease, Cardiovascular Research (2009) 84, 182–189.

49. Giorgio Baroldi, Riccardo Bigi and Lauro Cortigiani, Ultrasound Imaging Versus Morphopathology in Cardiovascular Diseases: The Heart Failure, Cardiovascular Ultrasound 2007, 5:5.

50. A. pantano, D. cerniglia, Simulation of laser generated ultrasound with application to defect detection, Appl. Phys. A 91, 521–528 (2008).

51. S. Dixon, S.E. Burrows, B. Dutton, Y. Fan, Detection of cracks in metal sheets using pulsed laser generated ultrasound and EMAT detection, Ultrasonics 51 (2011) 7–16.

52. C.T. Kwok, F.T. Cheng, H.C. Man, Synergistic effect of cavitation erosion and corrosion of various engineering alloys in 3.5% NaCl solution, Materials Science and Engineering A290 (2000) 145–154.

53. H. Ashassi-Sorkhabi, N. Ghalebsaz-Jeddi, Effect of ultrasonically induced cavitation on inhibition behavior of polyethylene glycol on carbon steel corrosion, Ultrasonics Sonochemistry 13 (2006) 180–188.

54. N.L.P.A. De Morais and C.M.A. Brett, Influence of power ultrasound on the corrosion of aluminium and high speed steel, Journal of Applied Electrochemistry 32: 653–660, 2002.

55. Ronggu-ang Wang, Influence of ultrasound on pitting corrosion and crevice corrosion of SUS304 stainless steel in chloride sodium aqueous solution, Corrosion Science 50 (2008) 325–328.

56. Richard C. Alkire and Stephen Perusich, The effect of focused ultrasound on the electrochemical passivity of iron in sulfuric acid, Corrosion Science, vol 23, No. 10, pp. 1121-1132, 1983.

57. Andreas Lindermeir, Christian Horst, Ulrich Hoffmann, Ultrasound assisted electrochemical oxidation of substituted toluenes, Ultrasonics Sonochemistry 10 (2003) 223–229.

58. Ji-Tai Li, Guo-Feng Chen, Wen-Zhi Yang, Tong-Shuang Li, Ultrasound promoted synthesis of 2-aroyl-1,3,5-triaryl-4-carbethoxy-4-cyanocyclohexanols, Ultrasonics Sonochemistry 10 (2003) 123–126.

59. F. Priego Capote &M. D. Luque de Castro, Ultrasound in analytical chemistry, Anal Bioanal Chem (2007) 387:249–257.

60. Michael E. Hyde, Richard G. Compton, How ultrasound influences the electrodeposition of metals, Journal of Electroanalytical Chemistry 531 (2002) 19-24.

61. Takashi Ohsaka, Motohiro Isaka, Katsuhiko Hirano, Tomoji Ohishi, Effect of ultrasound sonication on electroplating of iridium, Ultrasonics Sonochemistry 15 (2008) 283–288.

62. Huan-Yu Zheng, Mao-Zhong An, Electrodeposition of Zn–Ni–Al$_2$O$_3$ nanocomposite coatings under ultrasound conditions, Journal of Alloys and Compounds 459 (2008) 548–552.

63. Yu-Jun Xue, Hong-Bin Liu, Ming-Ming Lan, Ji-Shun Li, Hang Li, Effect of different electrodeposition methods on oxidation resistance of Ni–CeO2 nanocomposite coating, Surface & Coatings Technology 204 (2010) 3539–3545.

64. Simon Floate, Michael Hyde, Richard G. Compton, Electrochemical and AFM studies of the electrodeposition of cobalt on glassy carbon: an analysis of the effect of ultrasound, Journal of Electroanalytical Chemistry 523 (2002) 49–63.

65. Veronica Saez, Jose Gonzalez-Garcia, Jesus Iniesta, Angel FriasFerrer, Antonio Aldaz, Electrodeposition of PbO2 on glassy carbon electrodes: influence of ultrasound frequency, Electrochemistry Communications 6 (2004) 757–761.

66. Veronica Saez, Jose Gonzalez-Garcia, Jesus Iniesta, Angel FriasFerrer, Antonio Aldaz, Electrodeposition of PbO2 on glassy carbon electrodes: influence of ultrasound power, Electrochemistry Communications 4 (2002) 370–373.

67. Bruno G. Pollet, Jean-Yves Hihn, Timothy J. Masonc, Sono-electrodeposition (20 and 850 kHz) of copper in aqueous and deep eutectic solvents, Electrochimica Acta 53 (2008) 4248–4256.

68. Andrew J. Saterlay, Shelley J. Wilkins, Katherine B. Holt, John S. Foord, Richard G. Compton, and Frank Markenb, Lead Dioxide Deposition and Electrocatalysis at Highly Boron-Doped Diamond Electrodes in the Presence of Ultrasound, Journal of The Electrochemical Society, 148 (2) E66-E72 (2001).

69. B. Grysakowski, J.J. Jasielec, B. Wierzba, T. Sokalski, A. Lewenstam, M. Danielewski, Electrochemical Impedance Spectroscopy (EIS) of ion sensors Direct modeling and inverse problem solving using the Nernst–Planck–Poisson (NPP)

model and the HGS(FP) optimization strategy, Journal of Electroanalytical Chemistry 662 (2011) 143–149.

70. J.R. Dygas, M. Malys, F. Krok, W. Wrobel, A. Kozanecka, I. Abrahams, Polycrystalline BIMGVOX.13 studied by impedance spectroscopy, Solid State Ionics 176 (2005) 2085 – 2093.

71. Pahnit Seriburi, Shawn McGuire, Ashutosh Shastry, Karl F. Bohringer, and Deirdre R. Meldrum, Measurement of the Cell-Substrate Separation and the Projected Area of an Individual Adherent Cell Using Electric Cell-Substrate Impedance Sensing, Anal. Chem. 2008, 80, 3677–3683.

72. Sunil K. Roy, Mark E. Orazem, and Bernard Tribollet, Interpretation of Low-Frequency Inductive Loops in PEM Fuel Cells, Journal of The Electrochemical Society, 154 (12)B1378-B1388 (2007).

73. Byoung-Yong Chang and Su-Moon Park, Electrochemical Impedance Spectroscopy, Annu. Rev. Anal. Chem. 2010. 3:207–229.

74. Digby D. Macdonald, Reflections on the history of electrochemical impedance spectroscopy, Electrochimica Acta 51 (2006) 1376–1388.

75. M. Naito, N. Tanaka, and H. Okamoto, General relationship between complex impedance and linear stability in electrochemical systems, J. Chem. Phys., Vol. 111, No. 22, 8 December 1999.

76. Sunil K. Roy, Mark E. Orazem, and Bernard Tribolletb, Interpretation of Low-Frequency Inductive Loops in PEM Fuel Cells, Journal of The Electrochemical Society, 154 (12) B1378-B1388 (2007).

77. Sunil K. Roy and Mark E. Orazem, Error Analysis of the Impedance Response of PEM Fuel Cells, Journal of The Electrochemical Society, 154 (8) B883-B891 (2007).

PAPER

I. DEPOSITION OF CERIUM-BASED CONVERSION COATING ON ALUMINUM 380 ALLOY

C. Lin, S. Maddela, W. Fahrenholtz, M.J. O'Keefe

Materials Research Center, Department of Materials Science and Engineering,

Missouri University of Science and Technology, Rolla, MO 65409, USA

ABSTRACT

Cerium-based conversion coatings were deposited on as-cast aluminum 380 alloy substrates by a spontaneous immersion process. In this study, the effects of rinsing temperature prior to immersion in the coating deposition solution were studied with respect to the surface morphology, electrochemical response, and corrosion resistance of the coatings. Panels rinsed at 25°C prior to coating had large cracks and holes in the coating. In contrast, panels rinsed at 100°C prior to coating had a uniform coating morphology with fewer, smaller cracks. Electrochemical testing revealed that coatings deposited on substrates rinsed at 100°C had higher impedance (~80 k$\Omega\cdot$cm^2) and lower corrosion current (~0.34 µA/cm^2) compared to coatings deposited on substrates rinsed at 25°C, which had 10 k$\Omega\cdot$cm^2 impedance and 2.7 µA/cm^2 corrosion current. Finally, ASTM B117 salt spray testing showed that rinsing at 100°C prior to coating resulted in cerium-based conversion coatings that could resist the formation of salt tails for 8 days.

1. INTRODUCTION

Casting aluminum alloys are widely used in the automotive and aerospace industries where innovative, lightweight materials and product forms are needed to improve performance [1]. For cast metals such as the 3xx.x series aluminum alloys, the presence of Si and Cu leads to pitting corrosion, which can lead to the failure of aluminum alloy components [2].

Corrosion protection for a wide variety of aluminum alloy components is provided by coatings such as chromate conversion coatings. However, the toxicity and carcinogenic properties of hexavalent chromium (Cr^{6+}) [3] have caused severe restrictions to be imposed on the use of chromates. As a result, environmentally benign alternatives to chromates have been extensively investigated [4,5]. Potential replacements for chromate conversion coatings include anodized coatings [6], rare-earth-based inhibitors in conversion coatings [7], and sol-gel coatings [8]. Among potential chromate replacements, rare-earth inhibitors have attracted significant attention. Hinton et al. were the first to investigate cerium-based conversion coatings (CeCCs) as an environmentally benign alternative to chromate conversion coatings [9].

The corrosion resistance of CeCCs is thought to arise from a combination of barrier properties and active response to the environment. The barrier protection properties of CeCCs have been studied by changing processing parameters, specifically surface preparation [10], post-treatment [11], and the use of gelatin [12]. To optimize the corrosion resistance of CeCCs on high strength aluminum alloys, screening studies have been made [13]. The composition of the spray deposition solution used in the present

research is based on the optimal values identified by Geng et al, [13] that resulted in the best corrosion resistance on Al 2024-T3 alloy.

Previous study has focused on the deposition mechanisms of CeCCs from cerium chloride solutions onto aluminum alloy substrates. Hinton et al [14], speculated that many electrochemical cells would arise due to the different activities of intermetallic particles on the surface of an aluminum alloy when the alloy was immersed into the solution. When immersed, anodic dissolution would occur at different locations according to the inhomogeneous surface activity:

$$Al \rightarrow Al^{3+} + 3e^- \tag{1}$$

As Al dissolves, the corresponding cathodic reaction would be hydrogen evolution or the reduction of peroxide and/or oxygen dissolved in solution:

$$2H^+ + 2e^- \rightarrow H_2 \tag{2}$$

$$H_2O_2 + 2H^+ + 2e^- \rightarrow 2H_2O \tag{3}$$

$$O_2 + 4H^+ + 4e^- \rightarrow 2H_2O \tag{4}$$

The pH in the electrolyte near local cathodic sites increases as the electrode reactions proceed. At pH values lower than 2.5, H_2O_2 complexes with Ce(III) species in solution as $Ce(H_2O_2)^{3+}$, and with increasing pH values (2.5-3.3) through deprotonating steps peroxo species form $Ce(O_2)^{2+}$ and when the pH value reaches 6.5 $Ce(O_2)^{2+}$

transforms to $Ce(O_2)(OH)_2$ [15]. In the deposition process, H_2O_2 acts as a complexing agent, oxidant, crystallization inhibitor and OH^- generator [15].

The purpose of this paper is to investigate the deposition of cerium-based conversion coatings on cast AA380 alloy. The effects of pre-treatment and the temperature of the panel before immersion on coating morphology, electrochemical response and corrosion resistance were investigated.

2. EXPERIMENTAL PROCEDURE

AA380 alloy sheets 0.3 cm thick were cut into test panels 2.5 cm by 7.6 cm in size. Pretreatment of the panels prior to coating started with an isopropyl alcohol wipe followed by degreasing in an aqueous solution of a commercial alkaline cleaner (5 wt% Turco 4215 NC-LT in deionized water) for 5 minutes at 55°C. After degreasing, the panels were activated by immersion for 10 min at 60°C in an aqueous solution containing 1 wt.% sulfuric acid. Following cleaning and activation, the panels were rinsed in deionized water that was either at room temperature (nominally 25°C) or heated to 100°C. After rinsing, the panels were immersed in the deposition solution for different time intervals of up to 8 min.

The CeCC deposition solution was prepared from a stock solution consisting of 40 g $CeCl_3 \cdot H_2O$ (Alfa Aesar, 99.9%), 780 g of de-ionized water, pH adjusted to 2.07 with HCl. For the deposition solution, 205 g of the stock solution was mixed with 0.8 g of a water soluble gelatin (DSF, Rousselot) that was dissolved in 25 g of de-ionized water. Just before deposition, 15 ml of H_2O_2 (Fisher Chemical, 30 wt.%) was added.

Coated panels were post-treated by immersion for 5 minutes in a water solution containing 2.5 wt% Na_3PO_4 (pH adjusted to 4.5 with phosphoric acid) that was heated to

85°C. The corrosion resistances of the coated panels were evaluated using salt spray testing (Q-Fog, Q-Panel Lab Products) per ASTM standard B117. Panels with CeCCs were stored at room temperature in the laboratory for at least 24 h before characterization or salt spray testing.

The crystalline phases in the alloy and coatings were characterized by X-ray diffraction (Philips X-Pert Pro) using copper Kα radiation. Scanning electron microscopy (SEM; Hitachi S-4700) with energy dispersive X-ray spectroscopy (EDS; Phoenix System) was used to characterize the surface morphologies and compositions of CeCCs.

Electrochemical impedance spectroscopy (EIS) was carried out at open circuit potential with amplitude of 10 mV in the frequency range from 10^5 to 10^{-2} Hz. Measurements were made after stabilization in the test electrolyte for 1500 s. All experiments were conducted with a frequency response analyzer (Schlumberger SI 1255 HF) and a potentiostat/galvanostat (EG&G Princeton Applied Research Model 273A). Potentiodynamic analysis was carried out after EIS, the initial potential was -400 mV$_{SCE}$ and final potential is 800 mV$_{SCE}$ with respect to the open circuit potential, and the scan rate was 1mV/sec. The electrochemical cell was a 250 mL water jacketed beaker maintained at 25°C. The cell electrolyte was a modified prohesion solution, which consisted of 0.70 wt% $(NH_4)_2SO_4$ and 0.35 wt% NaCl in deionized water. The exposed area of the working electrode was 1 cm^2. A saturated calomel electrode (SCE) was used as the reference electrode and Pt mesh with an area of 12 cm^2 was used as the counter electrode.

3. RESULTS AND DISCUSSION

3.1. Effect of Pretreatment

X-ray diffraction analysis (not shown) of bare AA380 alloy detected five different phases, specifically the Al matrix phase, a second phase of Si, and three intermetallic phases that were present in trace quantities, Al_2Cu, $FeSi_2$ and $Al_{4.5}FeSi$. Combining analysis of surface morphology (Figures 1a and b) and EDS (not shown) of the substrate after pretreatment, it appears that $FeSi_2$ and/or $Al_{4.5}FeSi$ intermetallic particles were dissolved by the alkaline and acid pretreatment. Dissolution sometimes left holes in the substrates that were up to about 20 μm in diameter (Figures 1c and d).

Pretreatment also altered the electrochemical response of the substrates. From the potentiodynamic curves shown in Figure 2a pretreatment increased the open circuit potential from about -600 mV_{SCE} for the starting panel to about -500 mV_{SCE} after alkaline cleaning, acid activation and rinsing. Figure 2a also shows that the pretreatment increased the corrosion current from 0.3 $\mu A/cm^2$ before pretreatment to 2.0 $\mu A/cm^2$ after pretreatment. However, the rinsing temperature, 25°C or 100°C, did not produce significant differences in either the open circuit potential or the corrosion current. The increase in corrosion current after pretreatment indicates that the alloy surface is more electrochemically active and easier to coat. From the corresponding electrochemical impendence spectra, Figure 2b, the impedance of starting panel was around 40 $k\Omega \cdot cm^2$, which was much larger than the impedance after pretreatment (~7.5 $k\Omega \cdot cm^2$ for both rinsing temperatures). In comparison to previous studies [10], the pretreatment process likely reduced the thickness of the native oxide layer, which decreased the impedance of

the substrate. Previous analysis showed that the reduction in impedance and increase in corrosion current were necessary to promote deposition of CeCCs [10].

3.2. Electrochemical behavior of CeCCs

The substrates rinsed at 25°C prior to coating deposition, increasing the immersion time in the coating solution made the surface more electrochemically active. From the potentiodynamic curves in Figure 3a, the corrosion current increased from 0.82 $\mu A/cm^2$ after two minutes in the coating solution to 1.6 $\mu A/cm^2$ after 5 minutes and 2.7 $\mu A/cm^2$ after eight minutes (Table 2). In contrast, the open circuit potential did not vary significantly among the three panels, with all having values around -530 mV_{SCE}. The increasing corrosion current with the increasing immersion time suggests that the surface of the AA380 is more susceptible to chloride attack and dissolution. Therefore, the potentiodynamic curves for coatings on substrates rinsed at 25°C, increasing the immersion time appears to increase attack of the substrate by the coating solution.

For substrates rinsed at 100°C prior to coating deposition, increasing the immersion time in the coating solution increases the corrosion resistance. The potentiodynamic curves shown in Figure 3b reveal that the corrosion current decreased from 0.73 $\mu A/cm^2$ after immersion for 2 minutes to 0.54 $\mu A/cm^2$ after five minutes and to 0.34 $\mu A/cm^2$ after eight minutes (Table 2). The open circuit potential was about the same after immersion in the deposition solution for 2 or 5 minutes (-480 mV_{SCE}), but decreased to about -540 mV_{SCE} after immersion for eight minutes. The decreasing corrosion current indicated that the coatings had better corrosion resistance as the immersion time increased. Compared to panels rinsing at 25°C (0.82 $\mu A/cm^2$), rinsing at 100°C for 2 minutes resulted in a coating with better corrosion resistance (0.73 $\mu A/cm^2$) and the

corrosion resistance, as measured by corrosion current, continued to increase as deposition time increased. Therefore, rinsing at 100°C prior to coating deposition appears to be a better choice for deposition of CeCCs on AA 380.

The EIS results were consistent with potentiodynamic analysis. Rinsing at 25°C prior to deposition resulted in coatings with impedance values that decreased as immersion time increased (Figure 3c). For panels rinsed at 25°C prior to coating, the impedance was 32 kΩ•cm^2 after 2 minutes of immersion in the coating solution and the value decreased to 16 kΩ•cm^2 after 5 minutes and 10 kΩ•cm^2 after eight minutes. However, for panels rinsed at 100°C prior to coating deposition, the impedance was 36 kΩ•cm^2 after immersion in the coating solution for 2 minutes, and it increased to 49 kΩ•cm^2 after 5 minutes and 79 kΩ•cm^2 after 8 minutes (Figure 3d). For panels rinsed at 100°C prior to coating deposition, the impedance of 79 kΩ•cm^2 after 8 minutes of immersion in the coating solution was more than double the highest value for coatings deposited on panels rinsed at 25°C, which was 32 kΩ•cm^2 after 2 minutes of immersion in the coating solution. These results indicate that rinsing at 25°C prior to deposition led to corrosion resistance that decreased with increasing immersion time in the coating solution whereas rinsing at 100°C prior to coating deposition led to corrosion resistance that increased with the increasing immersion time.

3.3. Morphology and thickness of the CeCCs

Coatings that were deposited on panels rinsed at 25°C were cracked and had large holes. As shown in Figure 4, the cracks became larger as coating time increased. In addition to the cracks, large holes, ~5 μm in diameter were also observed on the panel surfaces. Even though the coatings were cracked, the average thickness (Figure 6) in

areas with coating increased as immersion time increased. For example, the coating thickness was about 350 nm after 2 min, but increased to nearly 2 μm after 8 min of immersion in the coating solution. However, the thickness was not uniform and varied across the panel. The surface morphology supports the electrochemical testing results that showed that the coating impedance decreased as immersion time increased for coatings on substrates rinsed at 25°C. The impedance approached a value of 10 kΩ•cm^2 for deposition times of 8 min, which was about one third of the value (32 kΩ•cm^2) after immersion for 2 minutes. Hence, SEM analysis is consistent with electrochemical results that showed that coatings deposited on substrates rinsed at 25°C did not serve as effective barriers to corrosion due to non-uniform coverage of the AA380 surface.

Coatings that were deposited on substrates that were rinsed at 100°C had a nodular appearance (Figure 5) similar to previous work [13]. The coatings covered the substrates and only a few, small cracks were observed. As with coatings on substrates rinsed at 25°C, the thickness of CeCCs deposited on substrates that were rinsed at 100°C is increasing with deposition time. After 2 minutes of immersion, the coating thickness was just over 200 nm and it increased to ~700 nm after immersion for 8 min (Figure 6). Despite being thicker than CeCCs on high strength aluminum alloys, such as Al 2024-T3 and Al7075-T6 [18, 19], the coatings had only a few small cracks. As shown by the electrochemical analysis in Figure 5c, coating impedance increased as immersion time increased, which is consistent with the formation of a thicker, continuous coating. Therefore, the surface morphology and thickness of the coatings are consistent with the electrochemical results, which showed that coatings on substrates that were rinsed at 100°C increased the impedance compared to uncoated substrates.

3.4. Corrosion Protection

Coatings had a yellow-gold appearance (Figures 7a and 8a) after post-treatment. Coatings deposited on substrate rinsed at 25°C prior to immersion showed a significant amount of white product corrosion after salt spray testing. Corrosion pits and salt tails were visible after 24 hours in salt spray testing as shown in Figure 7b. Coatings continued to degrade with further time in salt spray testing (Figures 7c and d). In contrast, coatings deposited on substrates rinsed at 100°C prior to deposition showed better corrosion resistance. After 24 hours, a few corrosion pits were present (Figure 8b), but significant salting was not observed until after 192 hours of salt spray testing. Therefore the results of salt spray testing were consistent with electrochemical characterization and surface morphology. Coatings deposited on substrates that were rinsed at 25°C prior to immersion had higher corrosion currents, lower impedance values, and were cracked, which led to more severe corrosion in salt spray testing. However, coatings that were deposited on substrates that were rinsed at 100°C prior to deposition had lower corrosion currents, higher impedance values, and were free of large cracks. As a result, coatings deposited on substrates rinsed at 100°C provided improved corrosion protection for AA380 alloy substrates.

4. CONCLUSION

Cerium-based conversion coatings were deposited on AA380 alloy substrates. This study examined the effect of changing the rinsing temperature prior immersion in the coating solution on the electrochemical response, coating morphology, and corrosion resistance of CeCCs. From the results described above, the conclusions that can be draw include:

(1): Differences in the rinsing temperature did not produce any noticeable differences in the morphology of the substrates prior to coating or the electrochemical response of the panels prior to coating. Pretreatment led to the removal of Fe and Si-rich intermetallic compounds from the substrate surfaces, but the open circuit potential (-500 mV$_{SCE}$), corrosion current (2 $\mu A/cm^2$), and impedance (7.5 k$\Omega \cdot cm^2$) of the pretreated panels were nearly identical regardless of the final rinsing temperature.

(2): Coatings deposited on panels rinsed at 25°C had cracks and large holes in the CeCCs. The cracks and holes became large and deeper with increasing immersion time. The surface morphology is consistent with results of the electrochemical tests. For example, immersion for 2 minutes resulted in a corrosion current of 0.82 $\mu A/cm^2$ and an impedance is 32 k$\Omega \cdot cm^2$. As the coating deposition time increased to 5 min, the cracks become bigger and large holes appeared, after 5 minutes immersion. This resulted in a corrosion current that increased to 1.6 $\mu A/cm^2$ and an impedance that decreased to 16 k$\Omega \cdot cm^2$. After 8 minutes of immersion in the coating solution, the coating had even lower values of corrosion current (2.7 $\mu A/cm^2$) and impedance (10 k$\Omega \cdot cm^2$).

(3): Rinsing at 100°C prior to coating deposition resulted in coatings that had uniform appearance and fewer cracks. With increasing immersion time, the thickness of the coatings increased, which enhanced the corrosion resistance. From electrochemical testing, immersion for 2 minutes in the deposition solution produced a corrosion current of 0.73 $\mu A/cm^2$ and an impedance of 36 k$\Omega.cm^2$ with a coating thickness of ~200 nm. Increasing the coating deposition time to 5 minutes increased the thickness of the coating to ~400 nm, decreased the corrosion current to 0.54 $\mu A/cm^2$, and increased the impedance to 49 k$\Omega \cdot cm^2$. Further increasing the immersion time to 8 minutes, increased

the coating thickness to ~750 nm, decreased the corrosion current to 0.34 $\mu A/cm^2$, and increased the impedance to 76 $k\Omega \cdot cm^2$.

(4): Cerium-based conversion coatings deposited on AA380 panels that were rinsed in water heated to 100°C after pretreatment but before CeCC deposition provided significant corrosion resistance. Whereas coatings deposited on substrates rinsed at 25°C had both pits and salt tails after only 24 hours in salt spray testing, coatings deposited on substrates rinsed at 100°C were able to inhibit formation of salt tails for at least 96 hours.

REFERENCES

1. J. Gilbert Kaufman, Elwin L. Rooy, "Aluminum Alloy Castings: Properties, Processes, and Applications," (Materials Park, OH: American Society for Materials International, 2004), pp.11, 69-71.

2. J.R. Davis, "Corrosion of Aluminum and Aluminum Alloys," (Materials Park, OH: American Society for Materials International, 1999), pp.11-12.

3. Sandra S. Wise, Julie H.C. Schuler, Amie L. Holmes, Spiros P. Katsifis, Michael E. Ketterer, Wendy J.Hartsock, Tongzhang Zheng, and John Pierce Wise, Sr, Comparison of Two Particulate Hexavalent Chromium Compounds: Barium Chromate Is More Genotoxic Than Lead Chromate in Human Lung Cells, Environmental and Molecular Mutagenesis 44,156–162 (2004).

4. H.J. Gibb, P.S.J. Lees, P.F. Pinsky and B.C. Rooney. Am. J. Ind. Med. 38 (2000), pp. 115.

5. S.M. Cohen. Corrosion, 51 (1995), pp. 71.

6. B. Meyers and S. Lynn, Surface engineering, In: ASM Handbook 5, ASM International, Materials Park, OH (1990), pp. 925–929.

7. Zhao Dan, Sun Jie, Zhang Lili, Tan Yong, Li Ji, Corrosion behavior of rare earth cerium based conversion coating on aluminum alloy, Journal Of Rare Earths, Vol. 28, 2010, pp. 371.

8. Giancarlo, R. Salazar-Banda, Sandra R. Moraes ,Artur J. Motheo , Sergio A. S. Machado, Anticorrosive cerium-based coatings prepared by the sol-gel method, J Sol-Gel Sci Technol (2009) 52,415–423.

9. B. R. W. Hinton, Corrosion inhibition with rare earth metal salts, Journal of Alloys and Compounds, 180 (1992) 15-25.

10. W. Pinc, S. Geng, M. O'Keefe, W. Fahrenholtz, T. O'Keefe, Effects of acid and alkaline based surface preparations on spray deposited cerium based conversion coatings on Al 2024-T3, Applied Surface Science, 255 (2009) 4061–4065.

11. Daimon K Heller, W. Fahrenholtz, M. O'Keefe, The effect of posttreatment time and temperature on cerium-based conversion coatings on Al 2024-T3, Corrosion Science, 52 (2010) 360–368.

12. W. Pinc, P. Yu, M. O'Keefe, W. Fahrenholtz, Effect of gelatin additions on the corrosion resistance of cerium based conversion coatings spray deposited on Al 2024-T3, Surface & Coatings Technology, 203 (2009) 3533–3540.

13. S. Geng , P. Yu , M. O'Keefe , W. Fahrenholtz ,T. O'Keefe, Screening study of spray solution parameters for depositing cerium-based conversion coatings on Al alloy 2024-T3, J Appl Electrochem, 40 (2010) 551–559.

14. B.R.W. Hinton, L. Wilson, Corros. Sci. 29 (1989) 967-975.

15. F.H. Scholes, C. Soste, A.E. Hughes, S.G. Hardin, P.R. Curtis, The role of hydrogen peroxide in the deposition of cerium-based conversion coatings, Applied Surface Science, 253 (2006) 1770–1780.

16. B. Rivera, B. Johnson, M. O'Keefe, W. Fahrenholtz, Deposition and characterization of cerium oxide conversion coatings on aluminum alloy 7075-T6, Surface and Coatings Technology, 176 (2004) 349–356.

17. C. S. Linz and S. K. Fang, Formation of Cerium Conversion Coatings on AZ31 Magnesium Alloys, Journal of The Electrochemical Society, 152 (2) B54-B59 (2005).

18. B. Treu, S. Joshi, W. Pinc, M. O'Keefe, and W. Fahrenholtz; Electrochemical and Structural Changes in Cerium-Based Conversion Coatings During Exposure to Salt Spray, Journal of The Electrochemical Society, 157 (8) C282-C287 (2010).

19. P. Jones, P. Yu, W. Pinc, M. O'Keefe, W. Fahrenholtz, and T. O'Keefe, Spray Deposition of Cerium Oxide-Based Conversion Coatings on Al 2024-T3, Int. J. Appl. Ceram. Technol., 5 [1] (2008)63–73.

Table 1. Compositions of Al alloy 380[1]

element	Si	Fe	Cu	Mn	Mg	Ni	Zn	Sn	Other	Al
wt%	7.5-9.5	2.0	3.0-4.0	0.50	0.10	0.50	3.0	0.35	0.50	balance

Table 2. Electrochemical parameters derived from Impedance and Potential measurement

Immersion Time (min)	Corrosion Parameters					
	R_p (k$\Omega \cdot$cm^2)		I_{corr} (μA/cm^2)		E_{corr} (mV$_{SCE}$)	
	25°C	100°C	25°C	100°C	25°C	100°C
2	32	36	0.82	0.73	-540	-480
5	16	49	1.60	0.54	-550	-480
8	10	76	2.70	0.34	-510	-540
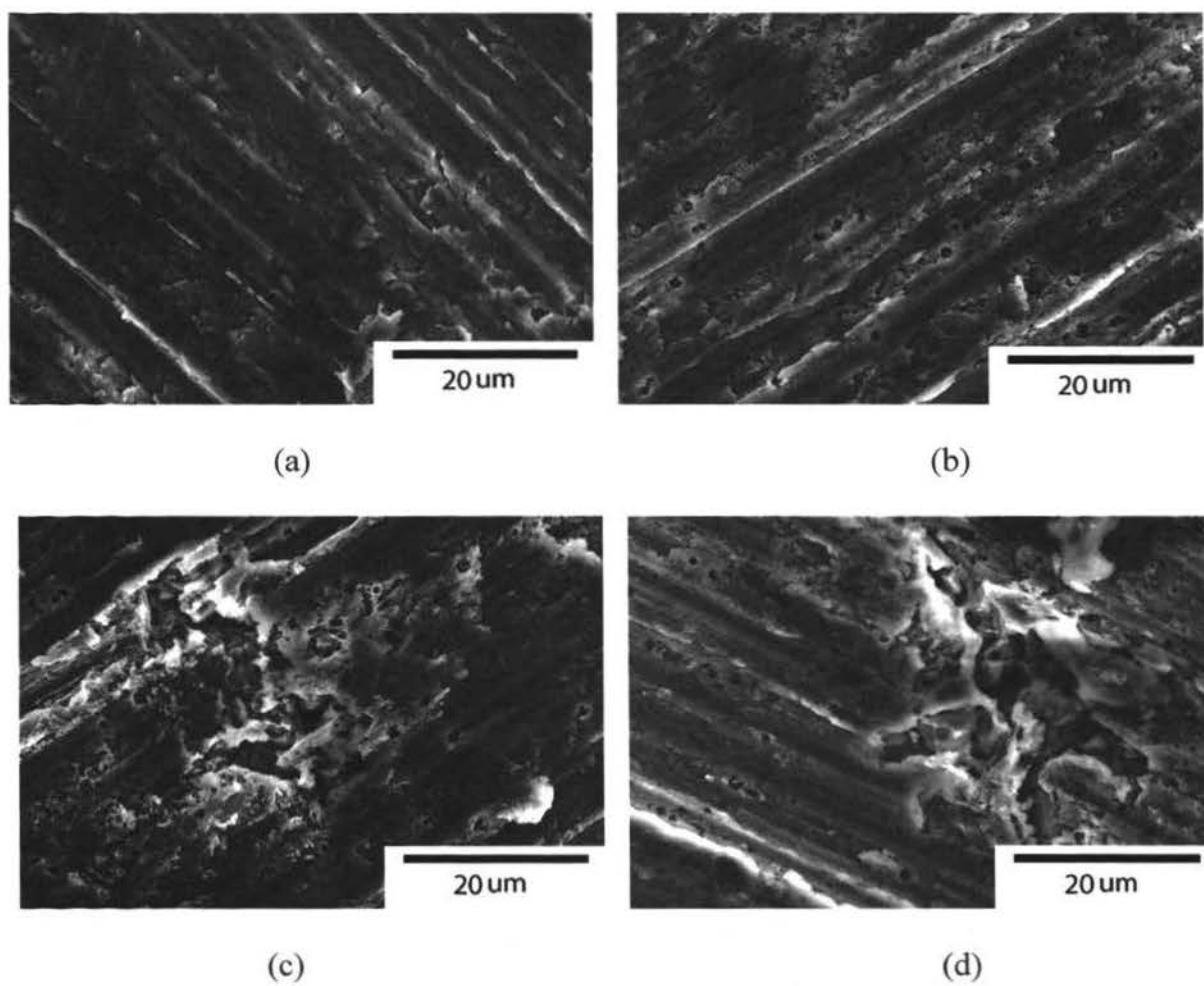
Figure 1. SEM surface morphology of AA 380 cleaned panel; a) 180 grit polished, b) 25°C rinsed, c) 25°C rinsed showing an area with removal of material; and d) 100°C rinsed.

(a)   (b)
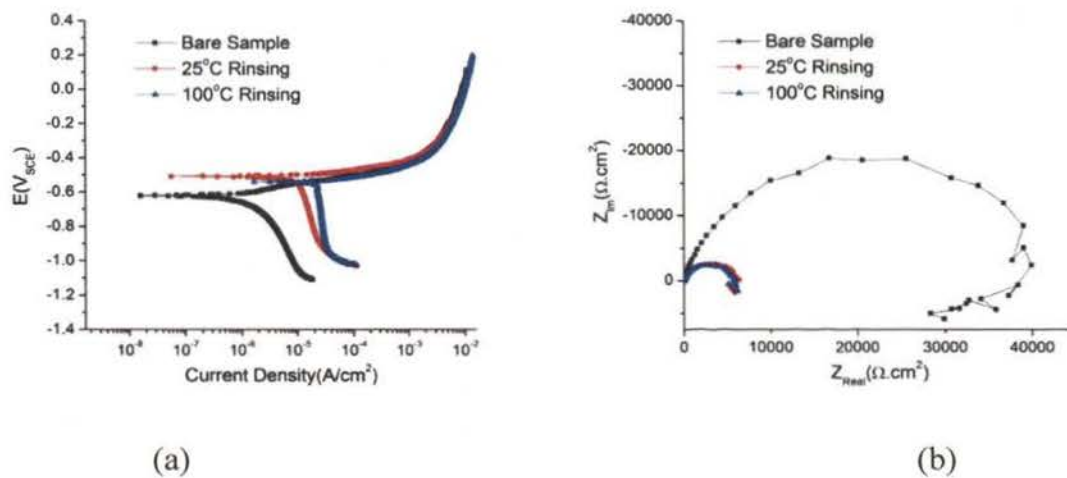
Figure 2. (a) Potentiodynamic polarization curves and (b) impedance spectroscopy of bare, rinsing at 25°C and 100°C of AA 380.

(a)

(b)

(c)

(d)
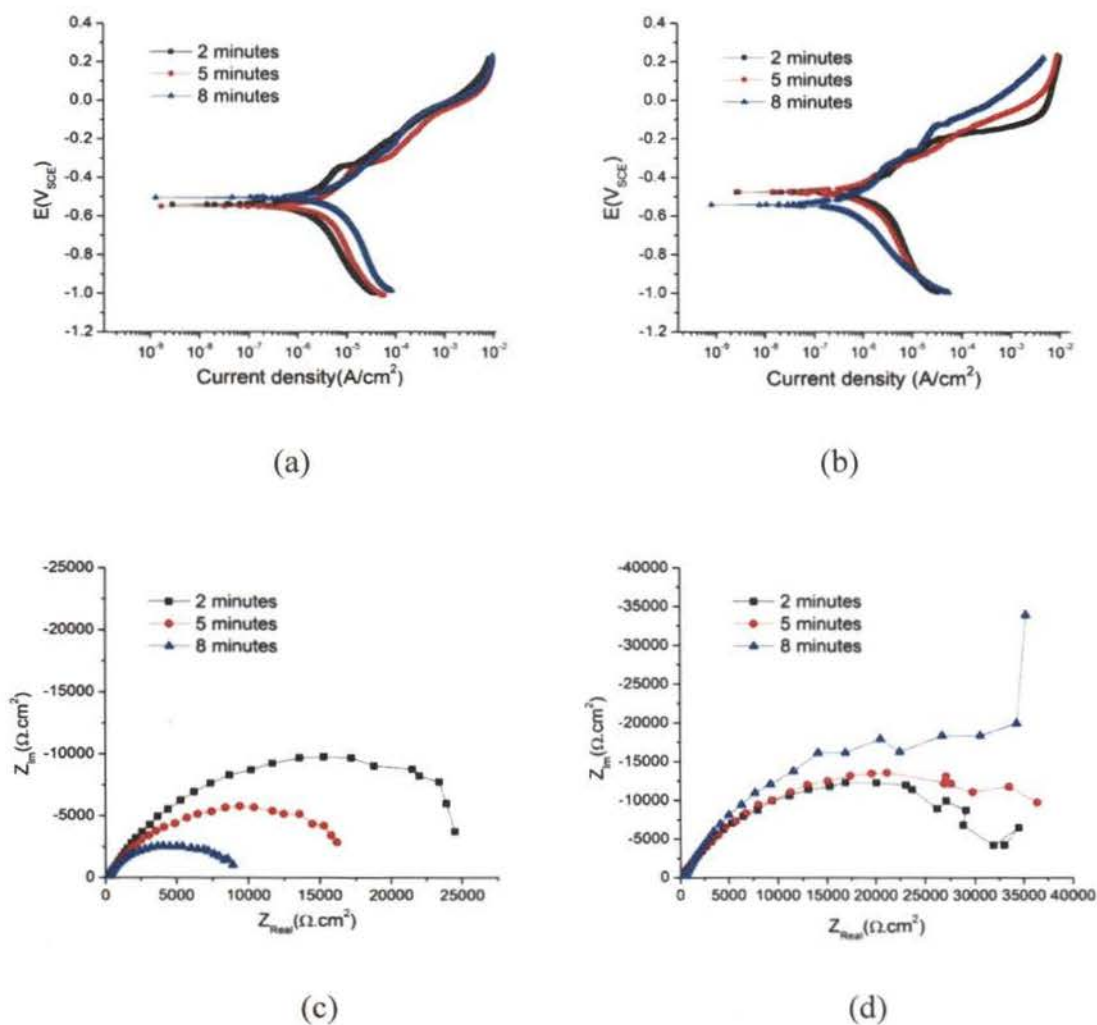
Figure 3. Electrochemical behavior of CeCCs deposited AA 380 in prohesion solution; potentiodynamic curve a) 25°C, b) 100°C, and impedance spectra, c) 25°C, and d) 100°C.

(a)

(b)

(c)
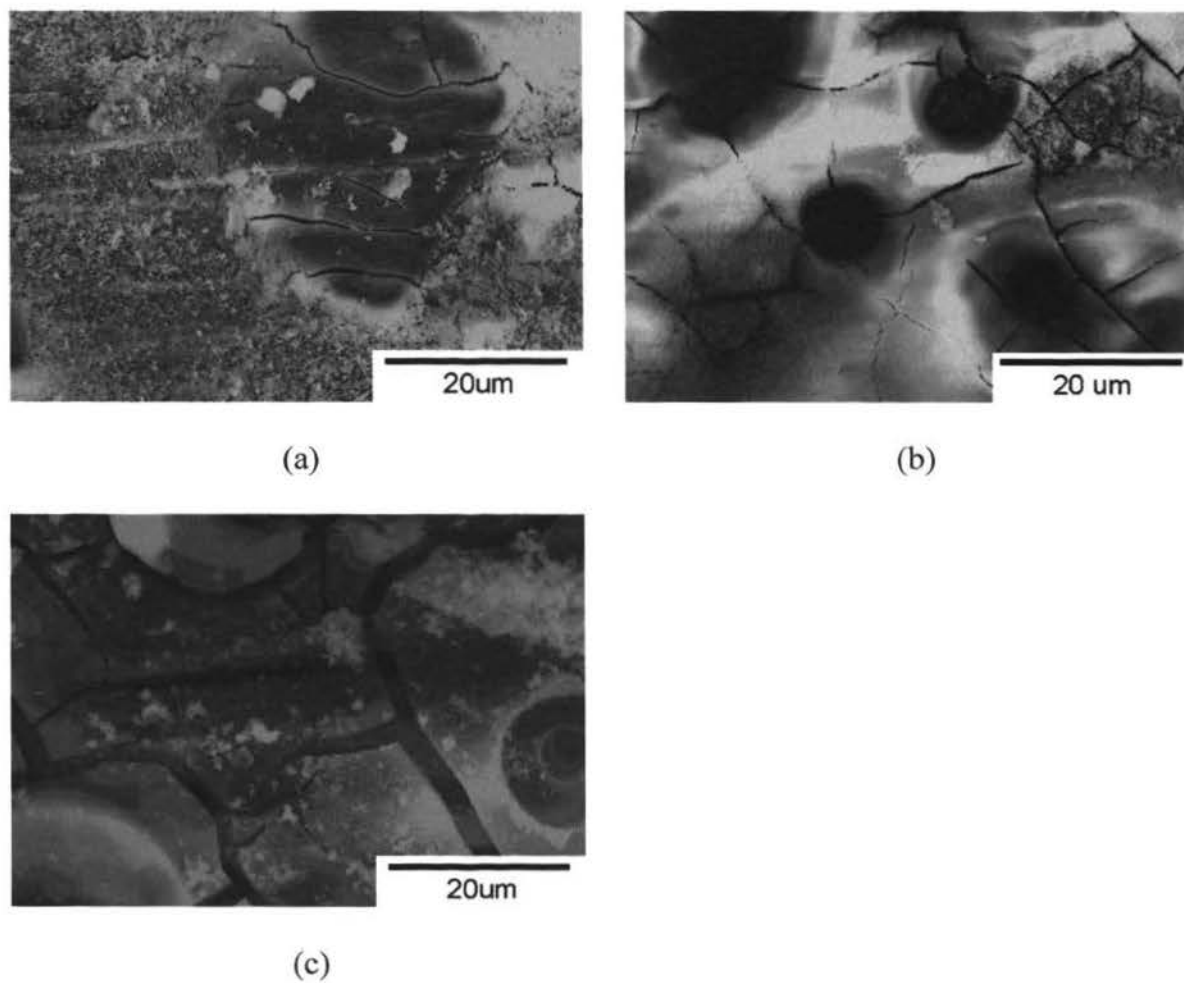
Figure 4. Surface morphology of coatings deposited on panels rinsed at 25°C after immersion in the coating solution; (a) 2 min, (b) 5 min, and c) 8 min.

(a)

(b)

(c)
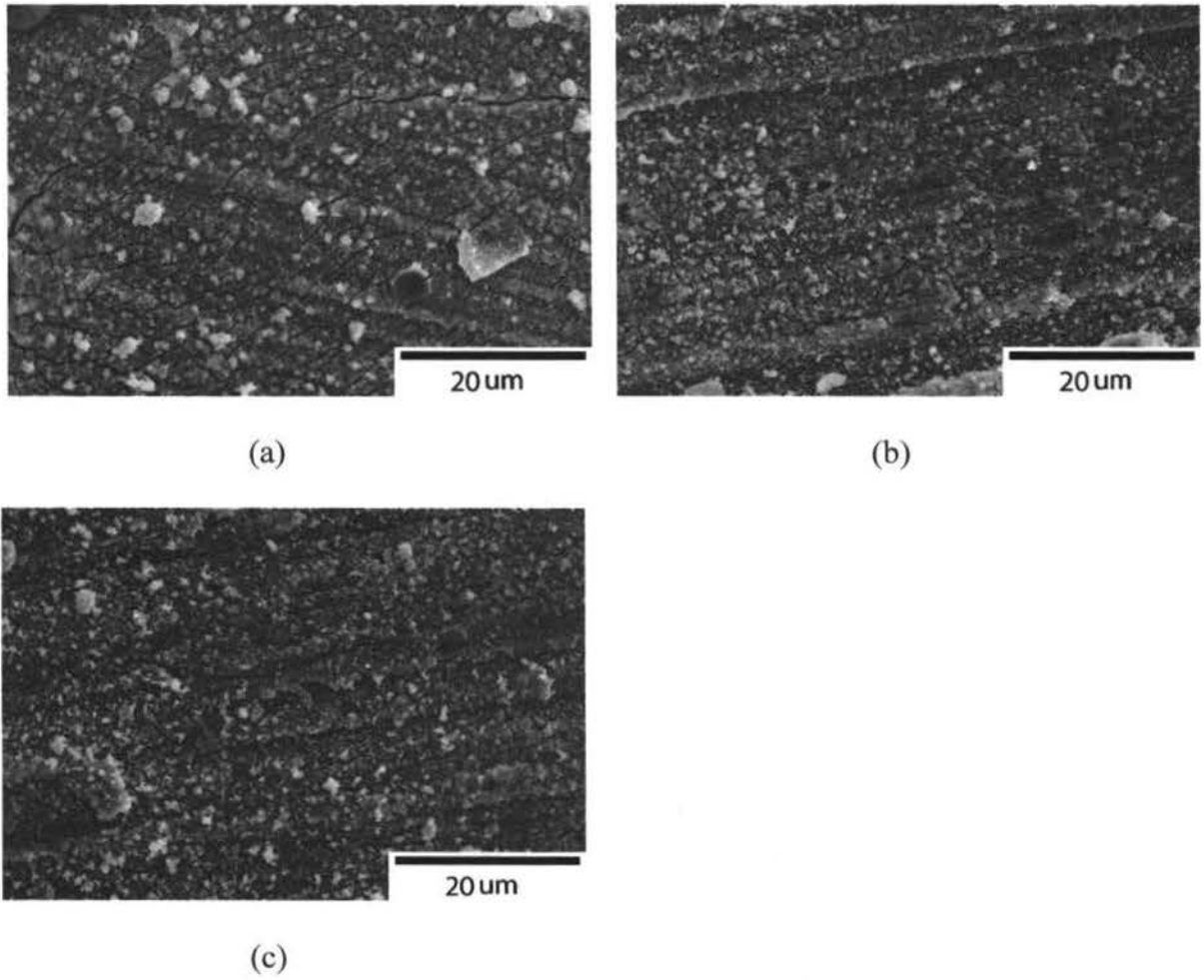
Figure 5. Surface morphology of coatings deposited on panels rinsed at 100°C after immersion in the coating solution; (a) 2 min, (b) 5 min, (c) 8 min.
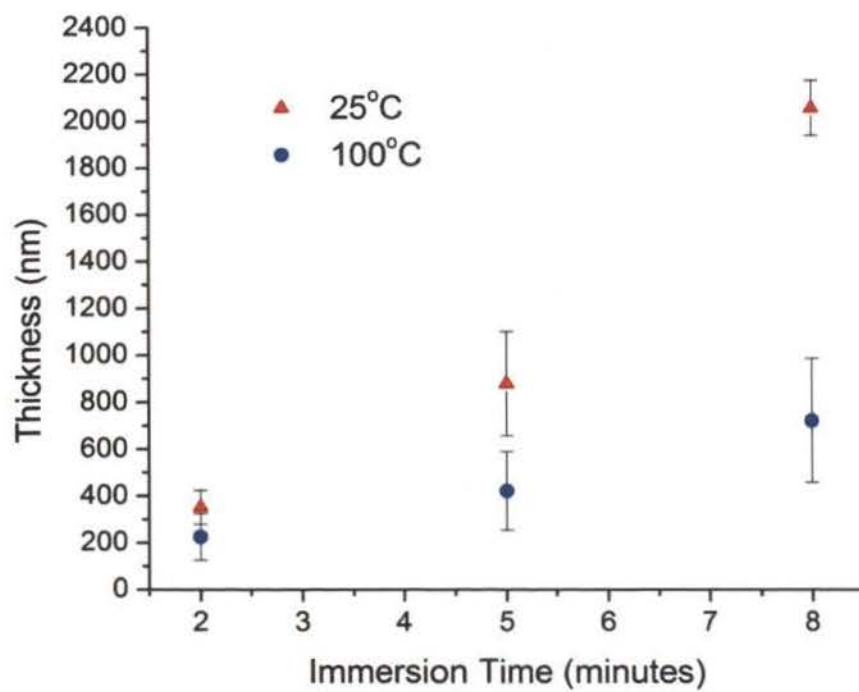
Figure 6. Thickness as a function of immersion time for CeCCs deposited on panels rinsed at 25°C and 100°C.
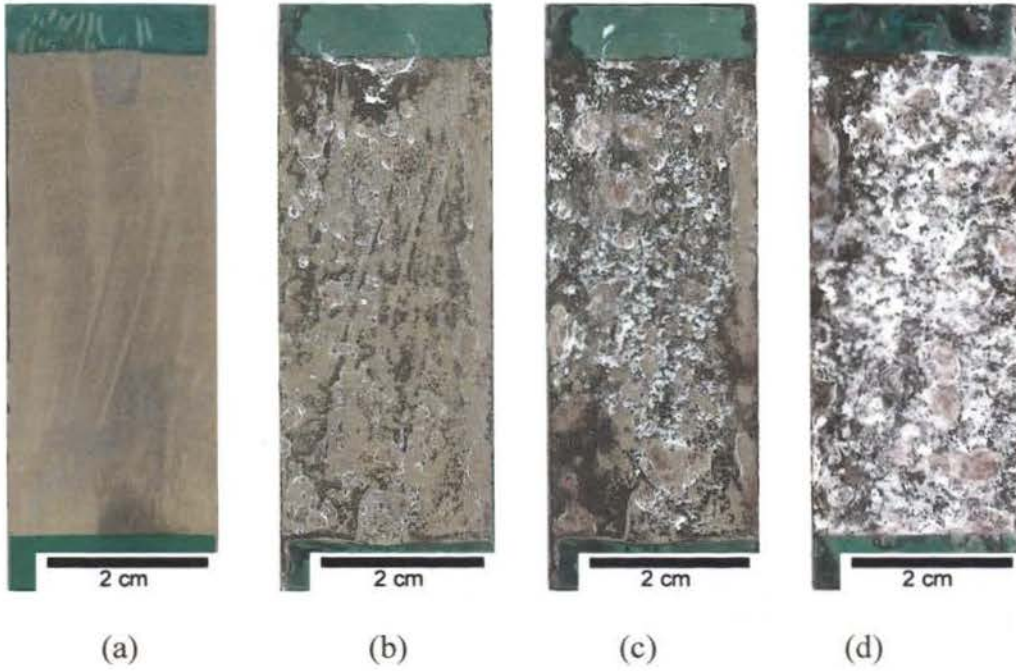
Figure 7. Optical images of coatings deposited on substrates rinsed at 25°C, a) as deposited, and after salt spray performance b) 24 hours, c) 96 hours, and d) 192 hours.
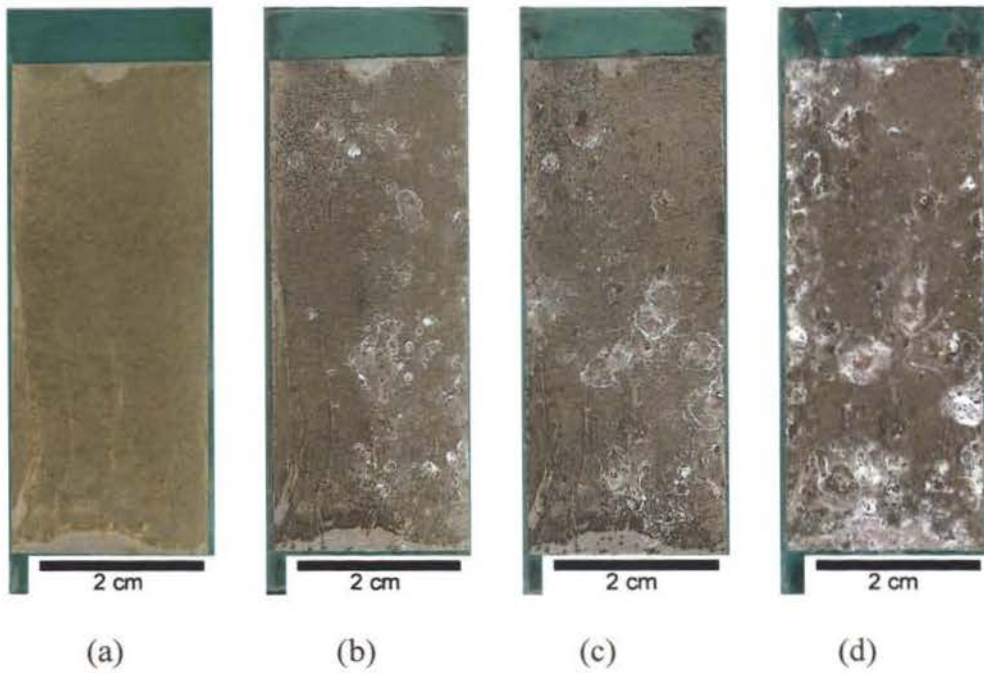
Figure 8. Optical images of coatings deposited on substrates rinsed at 100°C, a) as deposited, and after salt spray performance b) 24 hours, c) 96 hours, and d) 192 hours.

PAPER

II. CERIUM-BASED CONVERSION COATINGS DEPOSITED WITH

ULTRASONIC AGITATION

C. Lin, S. Maddela, William G. Fahrenholtz, Matthew J. O'Keefe

Materials Research Center, Department of Materials Science and Engineering,

Missouri University of Science and Technology, Rolla, MO 65409, USA

ABSTRACT

Cerium-based conversion coatings were deposited on aluminum 413 and 380 alloys by a spontaneous immersion process with ultrasonic agitation. The morphology of the coatings was affected by the orientation of panels during deposition. When the panels AA413 were horizontal in the ultrasound bath, two different kinds of morphology were observed; some areas had small cracks while other areas were free of cracks. The corrosion current on AA413 panels first decreased with increasing immersion time and then increased after 15 minutes immersion. When panels AA380 were oriented at 45 degrees to horizontal, uniform, crack-free coatings were obtained. The thickness of the coatings on AA380 was around 100 nm with ultrasonic agitation and 800 nm without agitation. However, electrochemical testing showed that coatings on AA380 deposited with ultrasound had a corrosion current 0.60 $\mu A/cm^2$ compared to 4.2 $\mu A/cm^2$ for a coating without agitation.

1. INTRODUCTION

Al-Si alloys are widely used due to their castability, high strength to weight ratio, corrosion resistance, etc.[1,2] In general, the resistance of aluminum alloys to corrosion in aqueous or atmospheric media is due to the rapid formation of a surface oxide film, which consists of α-Al_2O_3, $Al(OH)_3$, or $AlOOH$ phases[3,4]. However, the native oxide film on aluminum does not offer sufficient protection against aggressive anions. For example, the presence of chlorides or other halides results in pitting corrosion at local points on the alloy surface, which leaves the inner substrate exposed to media containing the aggressive anions [5,6]. To mitigate corrosion, chromate conversion coatings have been used to protect aluminum alloys [7,8,9]. However, chromates are carcinogenic, making them subject to increasingly stringent regulations. As a consequence, intense research efforts have been undertaken to find environmentally friendly compounds that act as corrosion inhibitors for aluminum alloys.

Rare earth metal conversion coatings have been investigated for the corrosion protection of high strength aluminum alloys. Rare-earth based coatings are an attractive alternative to chromate coatings. In particular, cerium compounds are non-toxic and are relatively inexpensive. To date, several methods have been used to form cerium-based conversion coatings on aluminum alloys [10–16].

Previous studies have focused on the deposition mechanisms of CeCCs from cerium chloride solutions onto a variety aluminum alloy substrates. Hinton et al. [17], speculated that many electrochemical cells would arise due to the different activities of intermetallic particles on the surface of an aluminum alloy when the alloy was immersed

into the solution. However, oxidants such as H_2O_2 reduce the deposition time and make CeCCs more attractive industrial utilization [18].

It is the attractive properties of ultrasound that make people concentrate on the effect of varied power and frequency on the deposition rate, morphology of the coating and the nucleation rate etc[19,20].The purpose of this paper is to investigate the effect of ultrasonic agitation on the deposition, properties, and corrosion protection of cerium-based conversion coatings.

2. EXPERIMENTAL PROCEDURE

Aluminum 413 (AA 413) and 380 (AA 380) alloy test panels were sectioned into 2.5 x 5.0 cm and 2.5 x 7.6 cm coupons from 0.3 cm thick sheets, respectively. The compositions of the alloys are summarized in Table 1. The test panels were prepared for coating deposition by polishing with 180 grit SiC paper and then wiping with isopropyl alcohol followed by degreasing in an aqueous solution of a commercial alkaline cleaner (5 wt.% Turco 4215 NC-LT in deionized water) for 5 minutes at 55°C. After degreasing, the panels were activated by immersion for 5 minutes (AA 413) or 10 minutes (AA 380) in an aqueous solution containing 1 wt% sulfuric acid that was heated to 80°C (AA 413) or 60°C (AA 380). Following cleaning and activation, the panels were rinsed with deionized water that was heated to 100°C. After rinsing, the panels were immersed in the deposition solution for different times up to 25 min. For some panels, ultrasonic agitation (Ultrasonik Cleaner, Model 28X, 45-49 kHz, NEY DENTAL INC.) was applied during deposition.

The CeCC deposition solution was prepared from a stock solution consisting of 40 g $CeCl_3 \cdot xH_2O$ (Alfa Aesar, 99.9%), and 780 g of de-ionized water with the pH

adjusted to 2.07 using HCl. For the deposition solution, 205 g of the stock solution was mixed with 0.6 g (AA 380) or 0.7 g (AA 413) of a water soluble gelatin (DSF, Rousselot) dissolved in 25 g of de-ionized water, and 20 ml of H_2O_2 solution (Fisher Chemical, 30 wt. % in H_2O). During deposition, some panels were placed horizontally in the coating bath while others were oriented so the panel was 45° from horizontal.

Coated panels were post-treated by immersion for 5 minutes in a water solution containing 2.5 wt. % Na_3PO_4 (pH adjusted to 4.5 with phosphoric acid) that was heated to 85°C. The corrosion resistances of the coated panels were evaluated using salt spray testing (Q-Fog, Q-Panel Lab Products) that was run according to ASTM standard B117. Panels with CeCCs were stored at room temperature in the laboratory for at least 24 hours before characterization or performance evaluation.

A dual beam system (Helios NanoLab 600, FEI) equipped with a focused ion beam (FIB) milling system and a scanning electron microscopy (SEM) column for imaging was used to prepare transmission electron microscope (TEM) specimens that were approximately 100 nm thick. The system employed a Ga ion source to selectively mill specimens so that a micromanipulator could lift out and mount TEM specimens onto Cu grids for subsequent analysis. Energy dispersive spectroscopy (EDS) was performed with a Noran EDS detector used on a Tecnai F20 STEM operated at 200 kV. The EDS data were used to identify trends in the composition of cross-sectional specimens and not as an exact quantitative measure of the specimen composition. The balance of reported compositional data consisted predominately of Cu (from the TEM mounting grid) but also of Ga (from FIB milling) and/or Pt (deposited to protect specimen surface during FIB milling).

Potentiodynamic polarization measurements were conducted using an EG&G 273A potentiostat (Princeton Applied Research, USA). A standard EG&G flat cell (Princeton Applied Research, USA) was used for electrochemical measurements. The cell was filled with a modified prohesion solution, which consisted of 0.70 wt% $(NH_4)_2SO_4$ and 0.35 wt% NaCl in deionized water. The exposed area of the working electrode was 1 cm^2. A saturated calomel electrode (SCE) was used as the reference electrode (RE) and Pt mesh with an area of 12 cm^2 was used as the counter electrode. Prior to electrochemical polarization, the open circuit potential (OCP) with time was monitored after immersion until a steady potential was obtained (~1500 s). Potentiodynamic polarization experiments were performed from −300 to 800 mV versus OCP with a scan rate of 1 mV/s. The corrosion current density (i_{corr}) was calculated from the potentiodynamic polarization plot by the Tafel extrapolation method. Electrochemical impedance spectroscopy (EIS) was carried out at open circuit potential with amplitude of 10 mV in the frequency range from 105 to 10-2 Hz. All experiments were conducted with a frequency response analyzer (Schlumberger SI 1255 HF) in conjunction with potentiostat/galvanostat (EG&G Princeton Applied Research Model 273A).

3. RESULT AND DISCUSSION

3.1. Coatings on AA 380

Electrochemical testing indicated large differences between the CeCCs deposited with and without ultrasonic agitation. Both potentiodynamic testing and electrochemical impedance analysis of coatings deposited on AA 380 revealed that the use of ultrasound (45° to the horizontal) improved the barrier properties of CeCCs (Figure 1a and b). Without ultrasound, potentiodynamic testing showed that the corrosion current was 4.2

$\mu A/cm^2$, compared to 0.60 $\mu A/cm^2$ for coatings deposited with ultrasound. In addition, the impedance of the coating deposited without ultrasound was 17.1 $k\Omega \cdot cm^2$, which was about one fifth of the impedance (88.9 $k\Omega \cdot cm^2$) recorded for the coating deposited with ultrasound. The coating deposited with ultrasound had a lower open circuit potential, which suggested that the surface of the coating deposited with ultrasound was more active than the other coating. Hinton and coworkers have reported that the decrease in OCP is indicative of a cathodic inhibition mechanism[21].Therefore coatings deposited using ultrasound are cathodically inhibiting aluminum surface compared to coatings deposited without ultrasound. Analysis of the potentiodynamic curves showed a passivation range of about 215 mV for a coating deposited without ultrasound compared to about 170 mV for a coating deposited with ultrasound. These results suggest that CeCCs deposited without ultrasound formed an effective barrier to chloride ions. However, the use of ultrasound during deposition results in higher impedance, lower corrosion current and higher activity, which indicated that using ultrasound during deposition, may provide a better compromise between the barrier properties of the coating and the activity of the panel, which may provide better corrosion resistance.

The surface morphology and thickness of CeCCs were affected by the utilization of ultrasound during deposition. Without ultrasound, the coatings had a nodular morphology with a network of small (<1 μm wide) cracks (Figure 2a). Examination of the coatings in cross section revealed that the thickness was around 800 nm (Figure 2b). In contrast, when ultrasound was used during deposition, the coating morphology appeared to be similar to the polished surface of the uncoated panels and no cracks were apparent (Figure 2c). FIB cross sections revealed that the coatings were only about 100

nm thick (Figure 2d), which was far less than the thickness of coatings deposited without ultrasound. Based on SEM analysis, the use of ultrasound affected both the coating thickness and morphology. Even though coatings deposited with ultrasound were thinner, the absence of cracks may be responsible for the increased impedance observed by electrochemical testing.

3.2. Coatings on AA 413

Coatings on aluminum alloy 413 were deposited in the horizontal orientation with ultrasound. Analysis of potentiodynamic curves and impedance spectroscopy (Figure 3) revealed that properties varied with immersion time. After deposition for 5 min, the corrosion current was 0.52 $\mu A/cm^2$ and the impedance was 49.9 $k\Omega \cdot cm^2$. When the immersion time was increased to 15 min, the corrosion current decreased to 0.29 $\mu A/cm^2$ with the impedance increasing to 89.3 $k\Omega \cdot cm^2$. Increasing the immersion time to 25 minutes led to an increase in corrosion current to 0.40 $\mu A/cm^2$ and a decrease in impedance to 65.2 $k\Omega \cdot cm^2$. Initially, the corrosion resistance was enhanced by increasing immersion time, but decreased as deposition time increased from 15 min to 25 min. From the potentiodynamic analysis, the curves reveal large passivation which indicates that the CeCCs provide a good protection for the panel AA 413. In addition, no pitting was visible after the electrochemical test. Therefore, 15 minutes appears to be the optimum time for ultrasound agitated CeCCs deposited on AA 413 substrate.

Coatings on AA 413 were thicker than those on AA 380 deposited using similar conditions. As shown in Figure 4, the thickness of a coating deposited AA 413 by immersion for 5 min with ultrasound was about 200 nm compared to about 100 nm for a coating deposited for 10 min on AA 380. During deposition, cavitation was observed on

the surface of the AA 380 panels, but not for AA 413 panels, which may mean that AA 380 is more sensitive to ultrasound than AA 413. From electrochemical testing (Figure 5), the ultrasound agitated CeCCs on AA413 panels that were deposited for ten minutes had a corrosion current of 0.41 $\mu A/cm^2$, and an impedance of 64 $k\Omega \cdot cm^2$,which were different compared to the panels AA 380 agitated for ten minutes in the cerium solution, Figure 5.

3.3. Morphology of the CeCCs on AA 413

The orientation of the panel during deposition affected both the surface morphology and electrochemical response. When panels were placed horizontally in the deposition bath, the coatings had a network of cracks that were ~500 nm wide on some areas of the surface (Figure 6a), while other areas appeared to be free of cracks (Figure 6b). However, when the panels were held at 45° in the ultrasonic bath, uniform coatings with fewer cracks were observed (Figure 4). The cracks in the coatings on AA 413 may be due to the thicker coating, which has been shown in previous studies [22] to lead to the development of cracks during drying.

The surface morphology of the coatings did not change noticeably with immersion times of 5 to 15 min. Coatings had similar nodule sizes (~ 100 nm) and crack widths (~100 nm) for immersion times of 5 minutes and 15 minutes, Figure 7. However, increasing the coating immersion time to 25 minutes resulted in larger cracks (>1 μm wide) compared to shorter immersion times, probably due to increased coating thickness. The coating morphology analysis is consistent with the electrochemical test results. For deposition times of 5 or 15 minutes, the morphologies of the coatings were similar. In this regime, increasing the deposition time increased the impedance, most likely due to an

increase in coating thickness. In contrast, for a deposition time of 25 minutes, large (>1 µm wide) cracks formed in the coating, which increased the corrosion current and decreased the impedance. Therefore, optimization of corrosion resistance requires balancing immersion time and morphology.

3.4. Cross section of CeCCs on AA 413

Cross sections of areas with different coating morphologies were examined. From a cross section in an area with a large (>1 µm wide) crack, a subsurface crevice was observed (Figure 8a). Previous studies have concluded that crevices in high strength aluminum alloys were formed due to the combination of H_2O_2 and chloride ions in the coating solution [23,24]. Based on this observation, casting alloys are also susceptible to the formation of subsurface crevices. In contrast, areas without cracks appeared to be free of subsurface crevices (Figure 8b).

3.5. Interface Morphology

Interfaces between CeCCs and aluminum 413 alloy substrates were examined using transmission electron microscopy and selected area electron diffraction. Figure 9 shows a CeCC deposited on AA 413 with ultrasound. The coating thickness appears to be ~500 nm from the image, but is likely thinner due to distortion because of tilting of the specimen. Diffraction patterns collected from the as-deposited CeCCs revealed several different structures through the coating. The diffraction pattern from the coating near the interface with the substrate was a ring pattern, which indicates a nanocrystalline material. The most intense d-spacing is about 1.50Å, Figure 9b, which is consistent with the presence of $CeO_2 \cdot 2H_2O$. Near the outer surface, the coating appears to be nanocrystalline, where the most intense ring has a d-spacing of about 1.15Å, Figure

9c,which is consistent with the presence of $CePO_4 \cdot H_2O$. The final diffraction pattern was from the substrate, which appeared to be crystalline Al, Figure 9d. Based on this analysis, CeCCs deposited on cast aluminum alloys exhibit the same crystalline phases observed in CeCCs deposited on high strength aluminum alloys [25].

3.6. Corrosion Resistance

For AA 380 panels, the use of ultrasound resulted in noticeably thinner coatings. As shown in Figure 10a, a coating deposited without ultrasound had a yellow-gold color, which is typical of CeCCs. In contrast, only small areas of yellow-gold color were observed when ultrasound was used during deposition (panel was 45° to the horizontal), indicating a thinner coating (Figure 10c). In addition, the use of ultrasound affected corrosion resistance in salt spray testing. After 12 days in salt spray testing, the coating deposited without ultrasound had numerous pits and salt tails on the surface (Figure 10b). The coating deposited with ultrasound had fewer pits on the surface (Figure 10d), but still had significant salting.

Coatings deposited in the horizontal configuration were not uniform (Figure 11). Some areas were yellow-gold, while others appeared to be much thinner and had a gray-metallic appearance. Based on the inhomogeneity of the coatings, different part of the panels had different corrosion resistance. For panels immersed in the coating solution with ultrasound for five minutes, ten minutes or fifteen minutes, the corrosion resistance in the center part of the panels where the coatings were thicker appeared to be better than near the edges where the coatings were thinner. In general, immersing in the solution for fifteen minutes has appeared to produce the best corrosion resistance among these three conditions as no pitting or salt tails were observed in the center part of the panel after 17

days in salt spray testing. Thus, the result of the salt spray test is consistent with the electrochemical test and the morphology of the coating, which indicated that coatings deposited for 15 minutes with ultrasound had the best combination of favorable coating morphology and high impedance.

4. CONCLUSION

The effect of the use of ultrasound during deposition on the electrochemical response, morphology and corrosion resistance of CeCCs was investigated. Results from the investigation include:

(1): For aluminum 380 alloy, the use of ultrasound during deposition enhanced the corrosion resistance of the CeCCs. The corrosion current was 0.60 $\mu A/cm^2$ and impedance was 88.9 $k\Omega \cdot cm^2$ for coatings deposited with ultrasound; however the corrosion current of CeCCs deposited without ultrasound was 4.2 $\mu A/cm^2$ and the impedance was 17.1 $k\Omega \cdot cm^2$.

(2): For aluminum 380 alloy, CeCCs were thinner (~100 nm) and crack free coating when deposited with 45° to the ultrasound, while deposition without ultrasound resulted in thicker CeCCs (~800 nm) with cracks.

(3): Coating thickness and morphology was influenced by the orientation of the panels during deposition because of the orientation of the ultrasound source. When panels were horizontal during deposition in the ultrasonic bath, at least two different morphologies were observed. Some areas of the coating had networks of small cracks, while others were free of cracks. In contrast, coatings deposited on panels held at 45 degrees during deposition were uniform and free of cracks.

(4): With increasing immersion time for aluminum 413 alloy in the presence of ultrasound agitation, the corrosion current decreased from 0.52 $\mu A/cm^2$ after five minutes of immersion to 0.29 $\mu A/cm^2$ after 15 minutes immersion. However, increasing the deposition time to 25 min increased the corrosion current to 0.40 $\mu A/cm^2$. These indicate the corrosion resistance was enhance after 15 minutes of immersion, but then degraded after 25 minutes immersion.

(5): Microstructural analysis of the interface between CeCCs and aluminum alloy 413 substrates revealed that utilization of the ultrasound during deposition exhibit the same crystalline phases observed in CeCCs deposited on high strength aluminum alloys.

(6): Generally speaking, ultrasound agitation produced better CeCCs on AA 380 and AA 413 due to better surface morphology. Coatings were more uniform on AA 380 panels that were oriented at 45 degree during deposition, which resulted in better salt spray corrosion performance. However, uniform coatings were difficult to deposit on AA 413 in the horizontal configuration, which resulted in non-uniform corrosion response.

ACKNOWLEDGEMENTS

REFERENCES

1. L.F.Mndolfo, Aluminum Alloys: Structure and Properties, Butterworth, London, 1979.

2. S.G. Shabestari, S. Ghodrat, Mater.Sci.Eng A 467(2007) 150-158.

3. Rangel C M, Paiva T L, Daluz P P. Anticorrosion treatments for aluminum and aluminum alloys. European Symposium on Corrosion Inhibitor, 2000, 29(9) 507.

4. Bethencourt M, Botana F J, Cano M J. High protective, environmental friendly and short-time developed conversion coatings for aluminum alloys. Applied Surface Science, 2002, 189(1/2) 162.

5. Wang Zhenyao, Ma Teng, Han Wei, Yu Guocai. Corrosion behavior on aluminum alloy LY 12 in simulated atmospheric corrosion process. Trans. Nonferrous Met. Soc. China, 2007, 17 326.

6. Neil W, Garrard C. The corrosion behavior of aluminum silicon carbide composites in aerated 3.5% sodium chloride. Corrosion Science, 1994, 36(5) 837.

7. Sun J, Qi G C, Tan Y. Characterization of chromate conversion film on tinplate substrate by XPS and electrochemistry methods. Surf. Interface Anal., 2009, 41 449.

8. Liu Y, Skeldon P, Thompson G E, Habazaki H, Shimizu K. Chromate conversion coatings on aluminum-copper alloys. Corrosion Science, 2005, 47 341.

9. Kulinich S A, Akhtar A S, Susac D, Wong P C, Wong K C, Mitchell K A R. On the growth of conversion chromate coatings on 2024-Al alloy. Applied Surface Science, 2007, 253 3144.

10. X.W. Yu, C.W. Yan, C.N. Cao, Study on the rare earth sealing procedure of the porous film of anodized Al6061/SiCp, Mater. Chem. Phys. 76 (2002) 228–235.

11. B.Y. Johnson, J.E. Edington, M.J. O'Keefe, Effect of coating parameters on the microstructure of cerium oxide conversion coatings, Mater. Sci. Eng. A 361(2003) 225–231.

12. B.R.W. Hinton, D.R. Arnott, N.E. Ryan, The inhibition of aluminium alloy corrosion by cerous cations, Met. Forum 7 (1984) 211–217.

13. B.R.W. Hinton, Corrosion inhibition with rare earth metal salts, J. Alloy. Compd.180 (1992) 15–25.

14. A.E. Hughes, R.J. Taylor, B.R.W. Hinton, L.Wilson, XPS and SEM characterization of hydrated cerium oxide conversion coatings, Surf. Interface Anal. 23 (1995) 540–550.

15. F. Mansfeld, F.J. Perez, Surface modification of Al/15%SiC metal matrix composite in molten salts containing $CeCl_3$, Surf. Coat. Technol. 86–87(1996) 449–453.

16. A.L. Rudd, C.B. Breslin, F. Mansfeld, The corrosion protection afforded by rare earth conversion coatings applied to magnesium, Corros. Sci. 42 (2000) 275–288.

17. B.R.W. Hinton, L. Wilson, Corros. Sci. 29 (1989) 967-975.

18. F.H. Scholes, C. Soste, A.E. Hughes, S.G. Hardin, P.R. Curtis, The role of hydrogen peroxide in the deposition of cerium-based conversion coatings, Applied Surface Science, 253 (2006) 1770–1780.

19. Veronica Saez, Jose Gonzalez-Garcia, Jesus Iniesta, Angel FriasFerrer, Antonio Aldaz, Electrodeposition of PbO2 on glassy carbon electrodes: influence of ultrasound frequency, Electrochemistry Communications 6 (2004) 757–761.

20. Veronica Saez, Jose Gonzalez-Garcia, Jesus Iniesta, Angel FriasFerrer, Antonio Aldaz, Electrodeposition of PbO2 on glassy carbon electrodes: influence of ultrasound power, Electrochemistry Communications 4 (2002) 370–373.

21. Arnott, D. R., Hinton, B. R. W., Ryan, N. E., Cationic film-forming inhibitors for the corrosion protection of AA 7075 Aluminum Alloy in chloride solutions, Materials Performance 26 (1987) 42-47.

22. S. Geng , P. Yu , M. O'Keefe , W. Fahrenholtz ,T. O'Keefe, Screening Study of Spray Solution Parameters for depositing Cerium-based conversion coatings on Al alloy 2024-T3, J Appl Electrochem, 40 (2010) 551–559.

23. W. Pinc, S. Maddela, M. O'Keefe, W. Fahrenholtz, Formation of Subsurface Crevices in Aluminum alloy 2024-T3 during deposition of Cerium-based conversion coatings, Surface & Coatings Technology 204 (2010) 4095–4100.

24. Daimon K Heller, William G. Fahrenholtz, Matthew J. O'Keefe, Chemical and Structural Analyses of Subsurface Crevices formed during Spontaneous Deposition of Cerium-based conversion coatings, Materials Characterization 62 (2011) 1071-1075.

25. Daimon K Heller, William G. Fahrenholtz, Matthew J. O'Keefe, Cross-sectional Analysis of As-deposited and Post-treated Cerium-based Conversion Coatings on Al2024-T3, PH.D dissertation (2010) 72-89.

26. J. Gilbert Kaufman, Elwin L. Rooy, "Aluminum Alloy Castings: Properties, Processes, and Applications," (Materials Park, OH: American Society for Materials International, 2004), pp.11.

Table 1. Compositions of AA 413 and 380[26]

element	Si	Fe	Cu	Mn	Mg	Ni	Zn	Sn	Other	Al
AA 413	11.0-13.0	1.05	0.45	0.45	0.10	0.50	0.50	0.15	0.50	balance
AA 380	7.5-9.5	2.0	3.0-4.0	0.50	0.10	0.50	3.0	0.35	0.50	balance

Table 2. Electrochemical parameters derived from potentiodynamic polarization measurements for CeCCs on AA 380 and 413

Sample	Agitated or not	Immersion Time (minutes)	E_{corr} (mV$_{SCE}$)	i_{corr} (μA/cm^2)	Impedance (k$\Omega \cdot$cm^2)	Passivation Range(mV)
AA 380	yes	10	-589	0.6	88.9	167
	not	10	-476	4.2	17.1	217
AA 413	yes	5	-571	0.52	49.9	-
	yes	10	-536	0.41	63.8	-
	yes	15	-544	0.29	89.3	-
	yes	25	-540	0.40	65.2	-
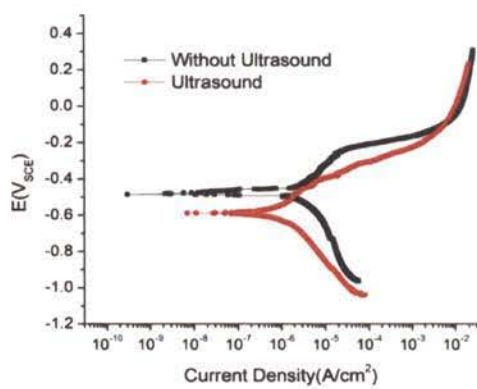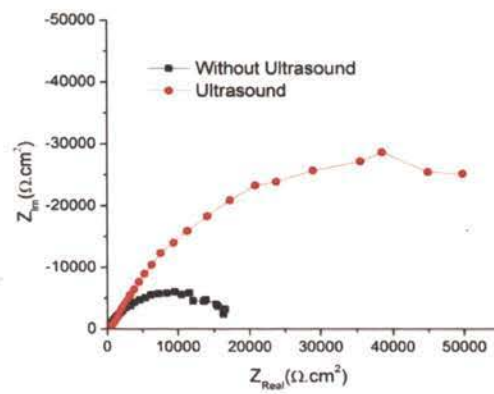
(a)   (b)

Figure 1. a) Potentiodynamic polarization, and b) electrochemical impedance spectra of CeCCs deposited on AA 380 with and without ultrasound.

(a)

(b)

(c)

(d)
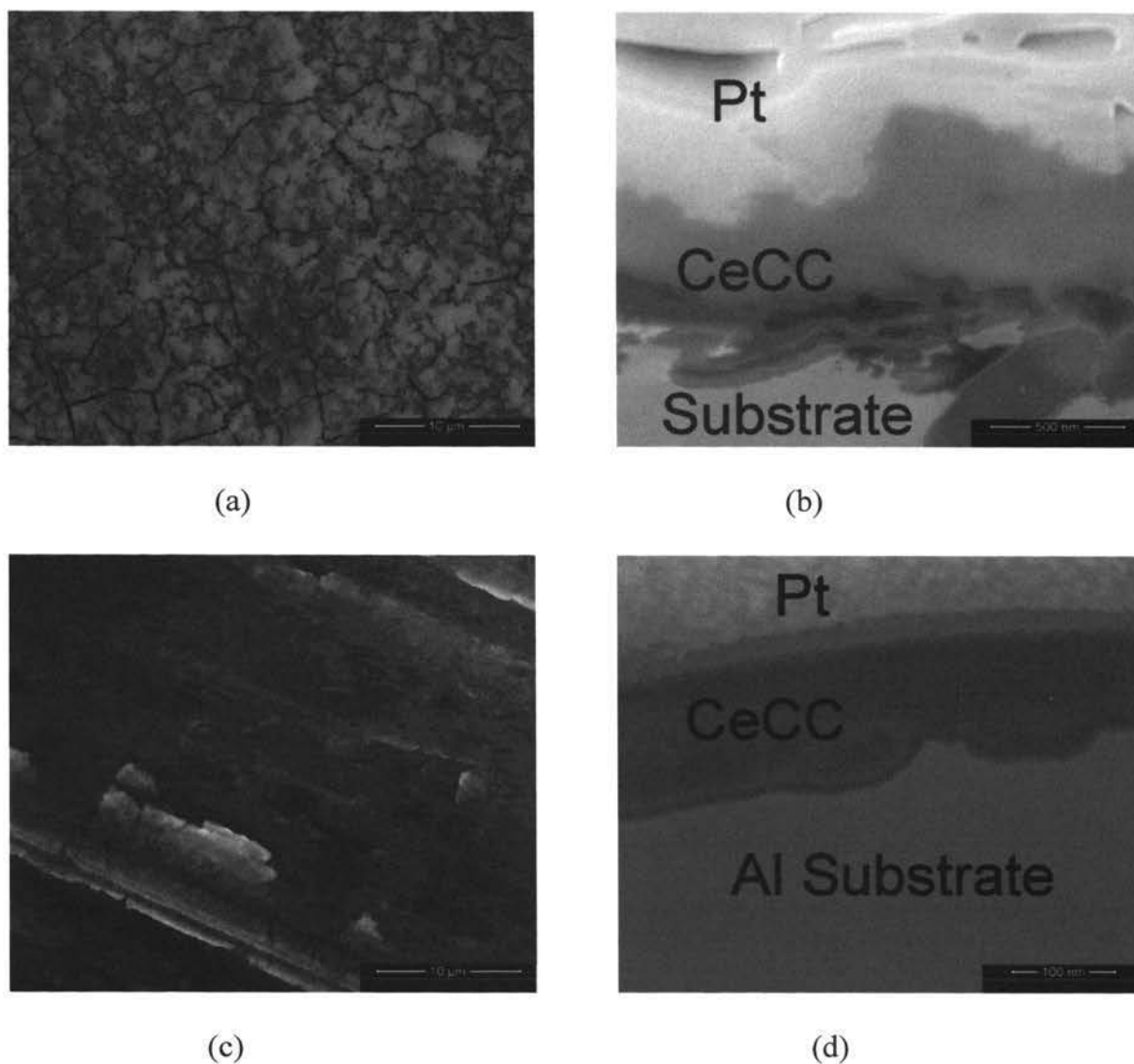
Figure 2. Images of CeCCs deposited on AA 380 without ultrasound; a) surface morphology, and b) cross-section, with ultrasound c) surface morphology, and d) cross-section. Note that the magnifications vary among the images.
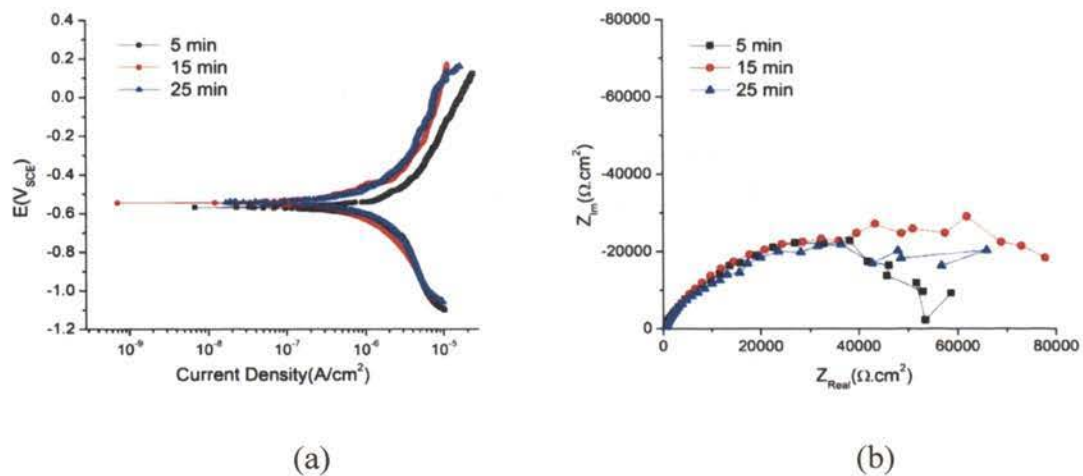
Figure 3. a) Potentiodynamic polarization, and b) electrochemical impedance spectra of CeCCs deposited on AA 413 under the ultrasound showing the effect of deposition time.

(a)

(b)
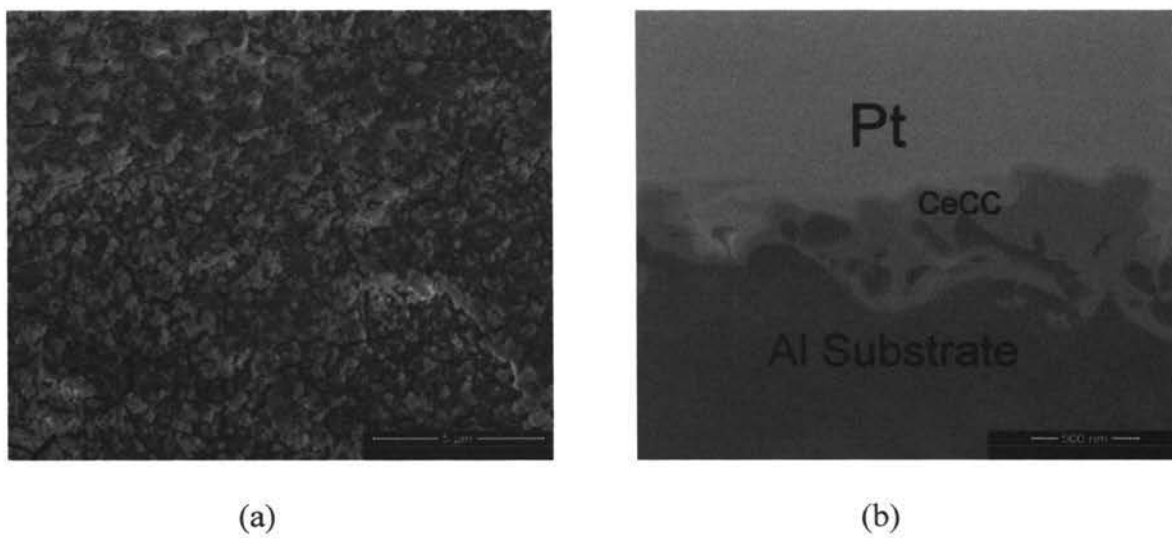
Figure 4. Coating morphology of CeCCs on AA 413 immersing for five minutes using ultrasound; a) surface morphology and b) cross-section.

(a)   (b)
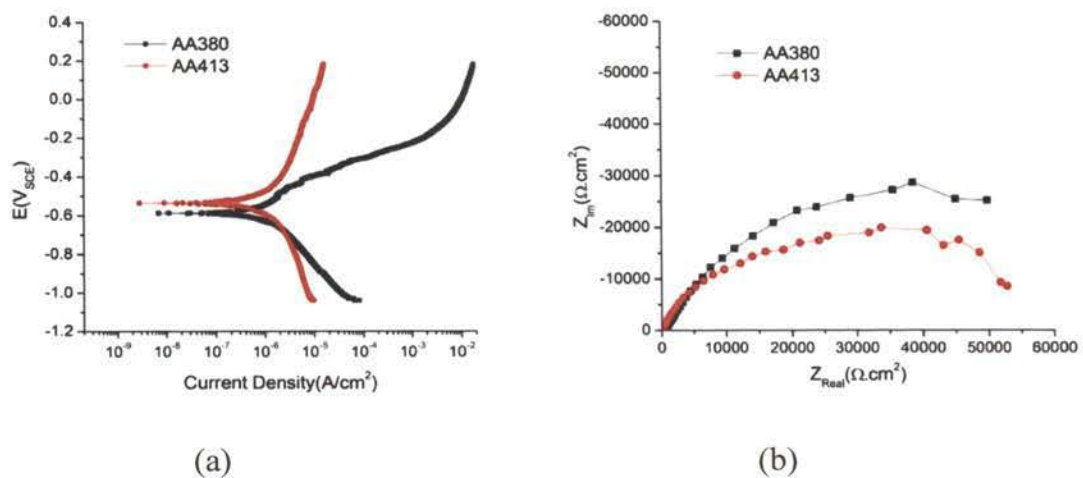
Figure 5. a) Potentiodynamic polarization and b) electrochemical impedance spectra of CeCCs on AA 413 and AA 380 with ultrasound agitated for ten minutes.

(a)   (b)
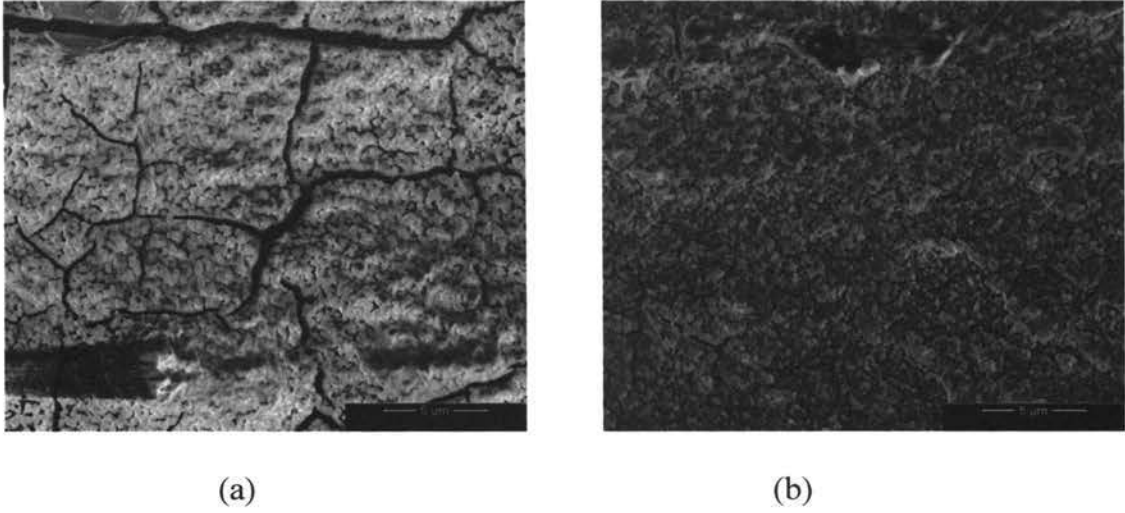
Figure 6. Surface morphology of CeCCs deposited on AA 413 horizontally in the ultrasound bath for 5 minutes; a) cracked region and b) a crack-free region.
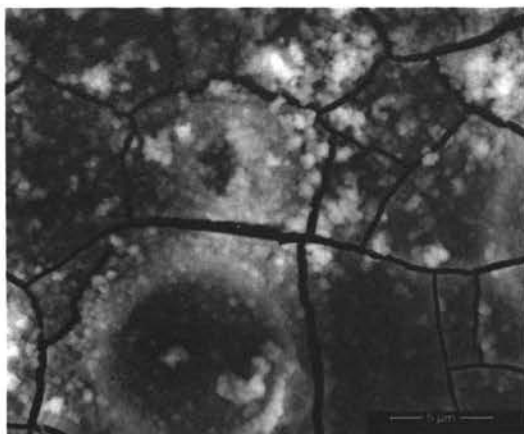
(a)
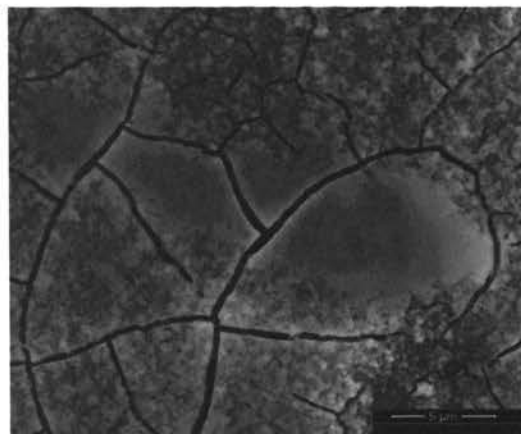
(b)
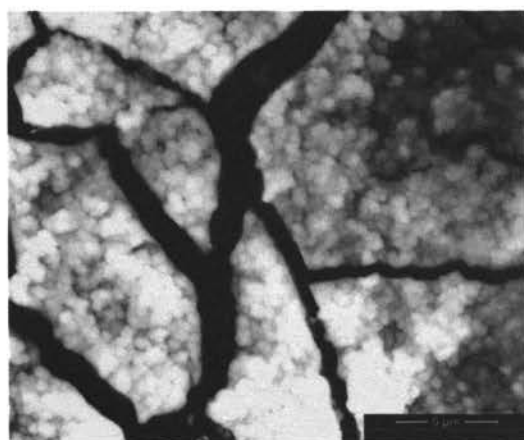
(c)

Figure 7. Surface morphology of CeCCs deposited on AA 413 agitated with ultrasound (a) 5 minutes , (b)15 minutes , (c)25 minutes.

(a)

(b)
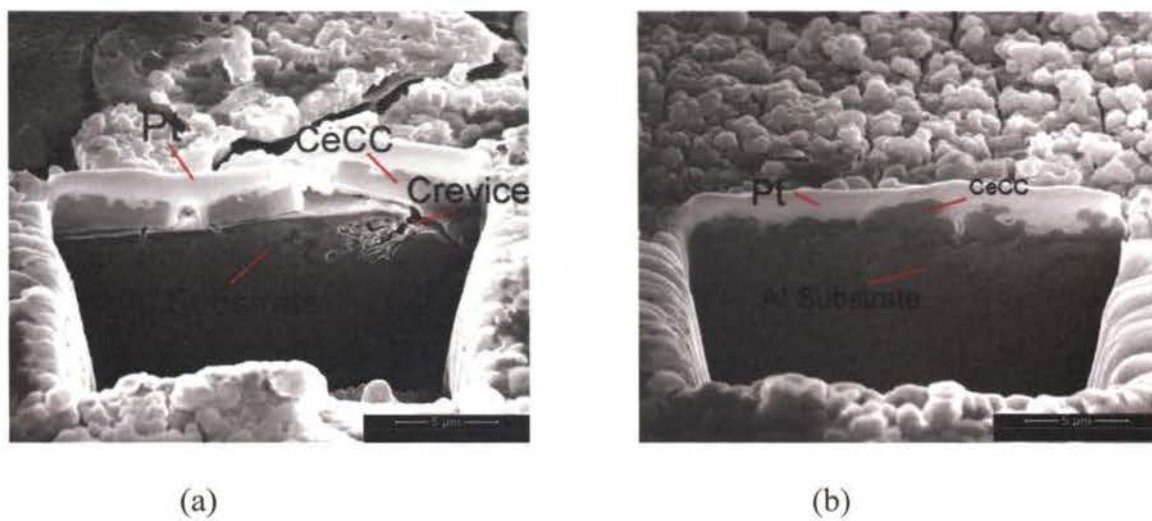
Figure 8. Cross-section of CeCCs deposited on AA 413 with immersion times of 25 minutes under the ultrasound; a) cracked region, and b) cracked-free region.

(a)
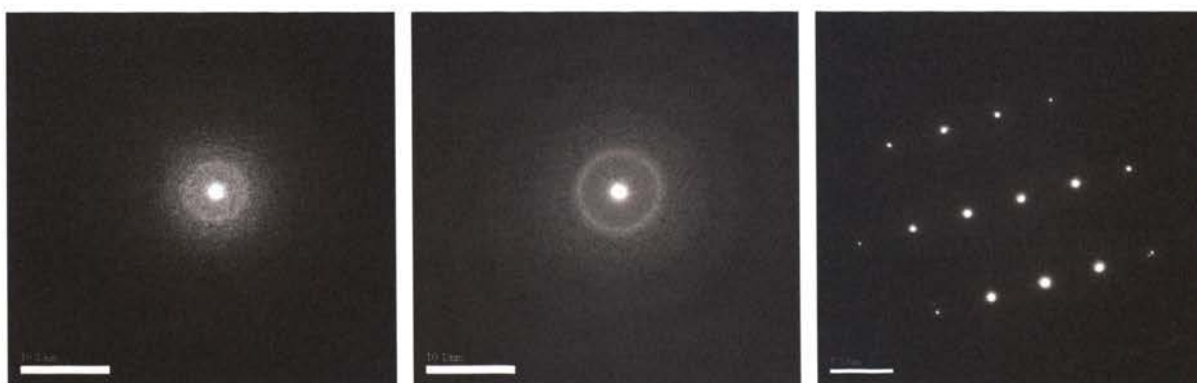
(b)   (c)   (d)

Figure 9. a) TEM image of the cross-section of a CeCCs on AA 413 using ultrasound bath, b) the diffraction pattern of the point b, c) point c, d) point d(matrix)
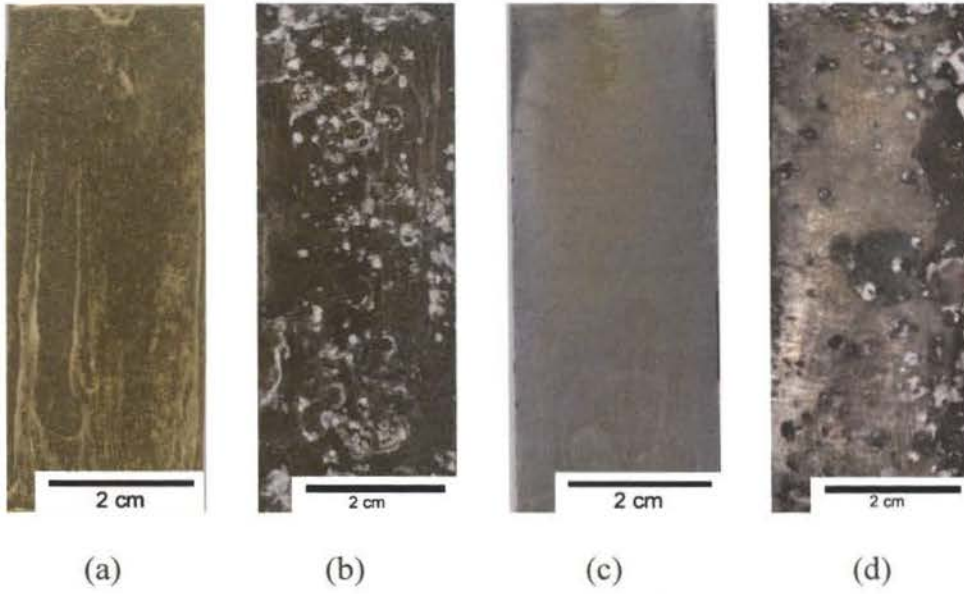
Figure 10. Optical image of CeCCs on AA 380 panels with immersion time 10 minutes; without ultrasound a) as-coated, b) 12 days salt spray, and with ultrasound 45° to horizontal c) as-coated, d) 12 days salt spray.
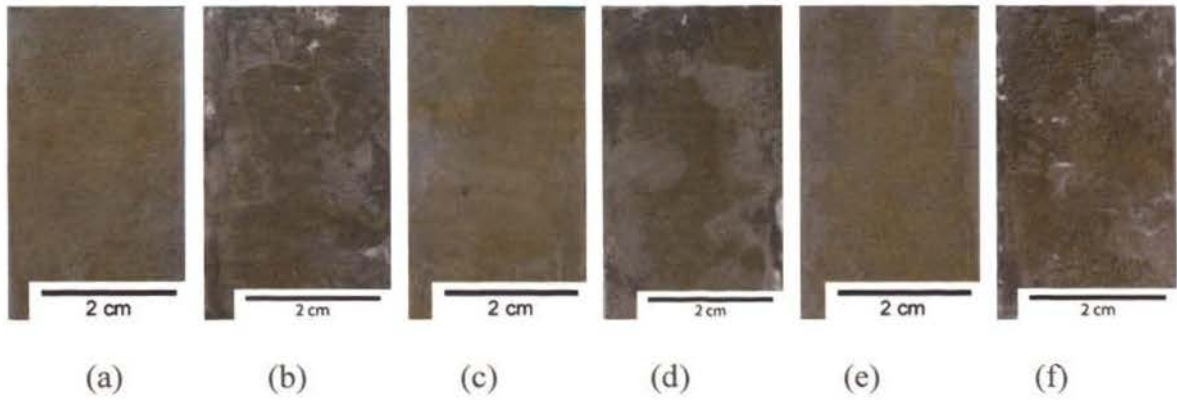
Figure 11. Optical images of as-coated and after 17 days salt spray tested cerium conversion coated AA 413 alloy panels deposited at different immersion time; 5 min a) as-coated, b) salt spray tested, 15 min c) as-coated, d) salt spray tested, and 25 min e) as-coated, f) salt spray tested.

SECTION

3. SUMMARY AND CONCLUSIONS

Cerium-based conversion coatings are a candidate for replacement of chromate conversion coatings. Previous experiments on high strength aluminum alloys 2024-T3 and 7075-T6 verify that CeCCs is an effective coating for resisting pitting corrosion when panels are exposed to chloride environments. This investigation deposited CeCCs on cast aluminum 380 and 413 alloys, which have different compositions and second phases than the high strength alloys.

Pretreatment plays an important role in the CeCC deposition procedure. The first paper describes the effect of rinsing temperature on electrochemical response, coating morphology and corrosion resistance of CeCCs. It turns out to be that high temperature rinsing resulted in better corrosion resistance and uniform coating morphology with fewer cracks and holes.

Electrochemical testing show that after pretreatment, the impedance of the panel was reduced from 40 $k\Omega \cdot cm^2$ to 7.5 $k\Omega \cdot cm^2$, and the corrosion current increased from 0.3 $\mu A/cm^2$ to 2.0 $\mu A/cm^2$. This indicates that after pretreatment, the thickness of the oxide layer is reduced, and more second phase is exposed to supply the driving force for the CeCCs deposited on the surface. The experiment result shows that rinsing at 100°C would cause uniformly thinner coating with fewer cracks than the coating rinsing at 25°C. After eight minutes immersion in the cerium solution, the panel rinsing at 100°C have impedance of 76 $k\Omega \cdot cm^2$, corrosion current 0.34 $\mu A/cm^2$, and can resist in the salt spray for eight days without visible salt tails. While at the same condition, the panel rinsing at 25°C has large cracks (> 5μm), and the impedance reduces to 10 $k\Omega \cdot cm^2$, corrosion

current was 2.7 $\mu A/cm^2$, and the coating was 2 μm thick, which could not resist salt spray for only one day without salt tails.

In order to further improve the efficiency of the CeCCs on Aluminum 380 and 413 alloys, the second paper investigated on how to change the structure and morphology of the CeCCs using ultrasound. AA 380 panel was very sensitive to the ultrasound due to the formation of cavitation, thus immersing the panel AA 380 45° to horizontal, obtaining a 100 nm thick, crack-free coating which has an 88.9 $k\Omega\cdot cm^2$ impedance, and could resist formation of salt tails for 12 days in salt spray testing. However, at the same condition, the normal coating has an 17.1 $k\Omega\cdot cm^2$ impedance, which was one fifth of the value for a coating deposited with ultrasound.

For panel AA 413, there are two kinds of morphology if we put the panel horizontal to the bottom, one has small cracks and the other is crack-free. Cross-sections showed places with cracks had thicker coating than the places where no crack was observed. Generally, after immersion in the solution for 15 minutes, the impedance was 89.3 $k\Omega\cdot cm^2$ and the corrosion current was 0.29 $\mu A/cm^2$.

4. SUGGESTION FOR FUTURE WORK

Based on the analysis presented in this thesis, future research on CeCCs should focus on developing mixture Pr and Ce conversion coating. This kind of conversion coating has different morphology and composition. Because of the synergic effect, this kind of conversion coating can have better corrosion resistance than singly cerium-based conversion coating. Different anti-corrosion mechanism can complement each other, which would make this kind of conversion coating more appropriate in a complex environment. With limited experiments on this kind of coating, the results show that the deposition mechanism and precipitation rates are totally different compared to cerium-based conversion coating. Optimization of processing parameters should be considered.

In order to obtain crack-free coating of appropriate thickness, ultrasound during deposition is attractive. CeCCs deposited with ultrasound have a lot of interesting characteristics which need more investigation to be explained, such as the thickness of the coating, the interface problem, the way the ultrasound acts on the panels and the electrochemical reaction under ultrasound.

APPENDIX A

UNPUBLISHED DATA FOR AA 413

IMMERSION TIME SELECTION
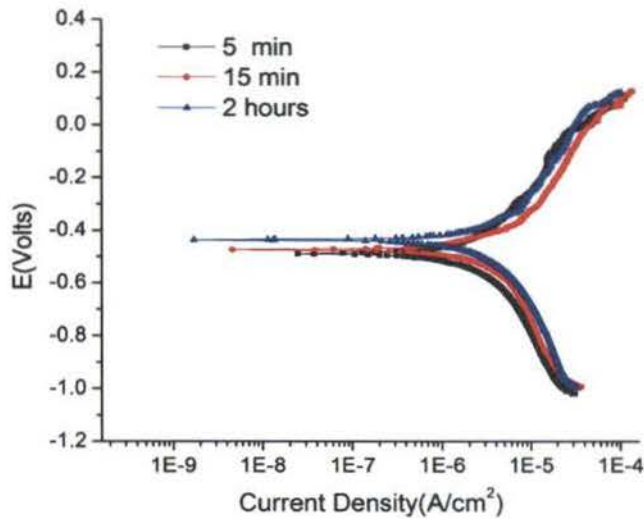
Figure A1. Potentiodynacmic curves of AA 413 immersing in the Cerium Solution for 5, 15, 120 minutes.

After five minutes 5wt% Turco solution at 55°C, and activated by 1wt% Sulfuric acid at 80°C for five minutes, the panels were immersed in the cerium solution for 5 minutes, 15 minutes and 120 minutes. The corrosion resistance decreased with increasing immersion time in this case. From the curves, it reveals that five minutes immersion the corrosion current was 0.98 $\mu A/cm^2$, and after 15 minutes, the corrosion current increased to 1.33 $\mu A/cm^2$. From immersion up to 120 minutes immersion, the corrosion current was still 1.32 $\mu A/cm^2$, figure A1.The changed in impedance of the CeCCs was consistent with the potentiodynamic curves. (Table A1)

Table A1. Electrochemical characterization results for CeCCs on AA 413

Immersion Time	E_{corr} (mV$_{SCE}$)	i_{corr} (μA/cm^2)	Impedance (k$\Omega\bullet$cm^2)
5 minutes	-490	0.98	26.7
15 minutes	-475	1.33	19.6
2 hours	-441	1.34	19.4

EFFECT OF ACTIVE SULFURIC ACID TEMPERATURE ON ELECTRO-DEPOSITION
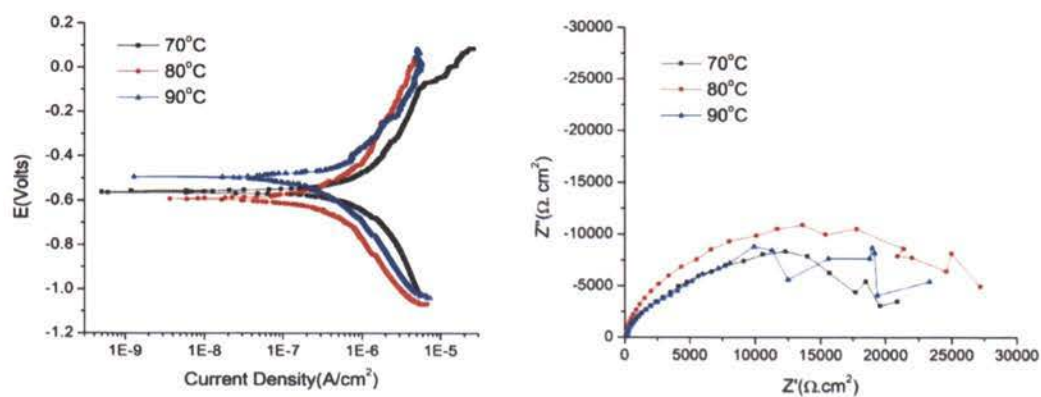
Figure A2. Potentiodynamic analysis and EIS of the CeCCs electrodeposited after different temperature sulfuric acid activation for five minutes.

Different temperatures of sulfuric acid activation have different effects on coating deposition. After alkaline cleaning in 5wt% Turco solution at 55°C for 10 minutes, activation at temperature 70°C in sulfuric acid for 5 minutes, then immersion in the Cerium solution for 5 minutes, the corrosion current of the CeCCs was 4.10 $\mu A/cm^2$, and impedance was 20.6 $k\Omega.cm^2$. But with activation at 80°C, the corrosion current of CeCCs was reduced to 2.38 $\mu A/cm^2$, and the impedance was 35.4 $k\Omega \cdot cm^2$. However, activation at 90°C in Sulfuric acid, corrosion current increased to 3.32 $\mu A/cm^2$, which impedance decreased to 25.4 $k\Omega \cdot cm^2$. Therefore, activation at 80°C in Sulfuric acid produced the best corrosion resistance among these three temperatures.

Table A2. Summary of electrochemical test results for CeCCs deposited on AA 413 after activation at different temperatures

Temperature	$E_{corr}(mV_{SCE})$	$i_{corr}(\mu A/cm^2)$	Impedance($k\Omega.cm^2$)
70°C	-560	4.10	20.6
80°C	-592	2.38	35.4
90°C	-504	3.32	25.4

APPENDIX B

UNPUBLISHED DATA FOR AA 380

EFFECT OF Ag ION ON THE ELECTRODEPOSITION OF CECCS
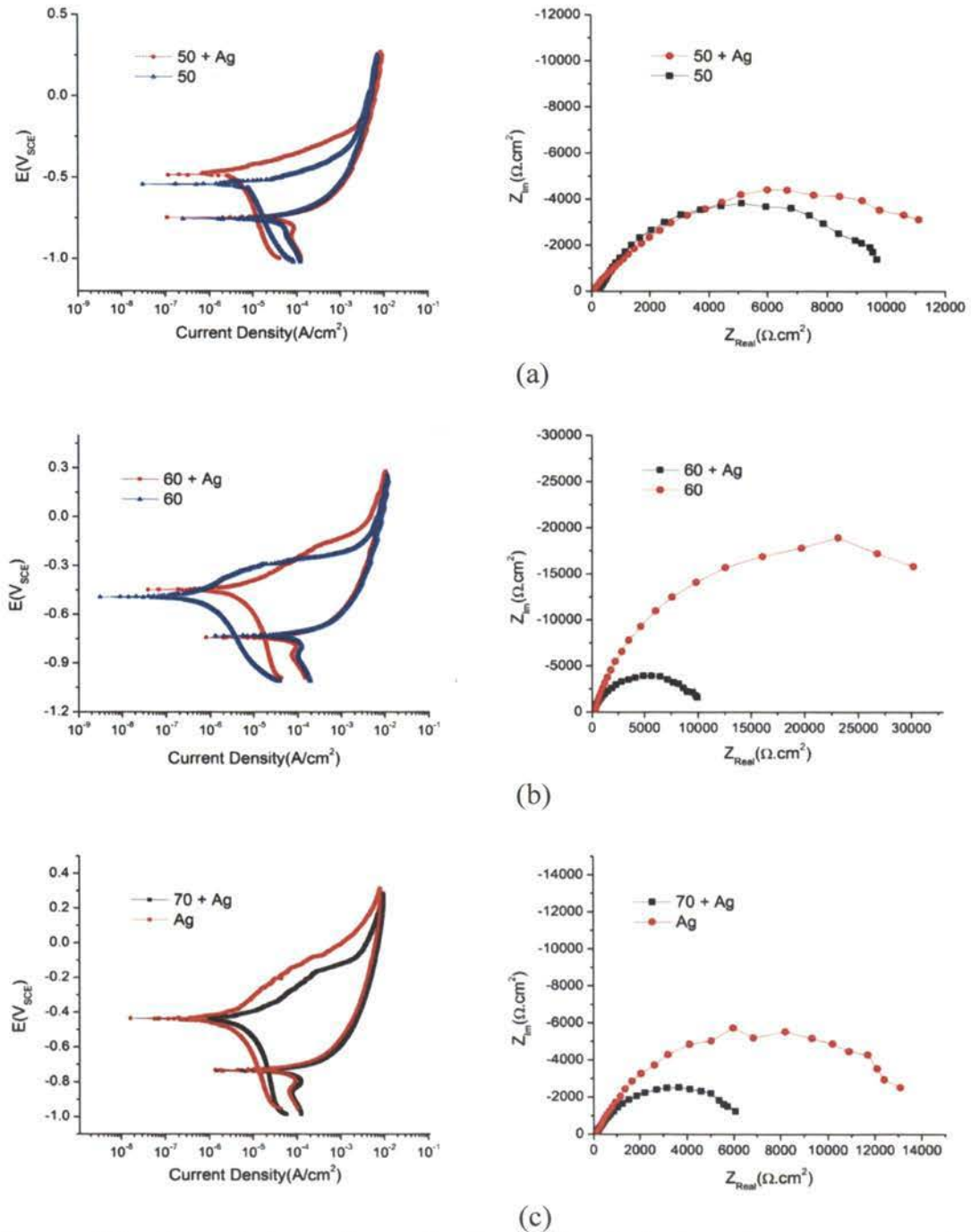
(a)

(b)

(c)

Figure B1. Potentiodynamic and electrochemical impedance curves for CeCCs electrodeposited with and without silver addition using the pretreatment of 5 minutes in 5wt.% Turco solution at 55°C, and then 5 minutes in 1wt.% Sulfuric acid at a) 50°C, b) 60°C, c) 70°C, d) 80°C.
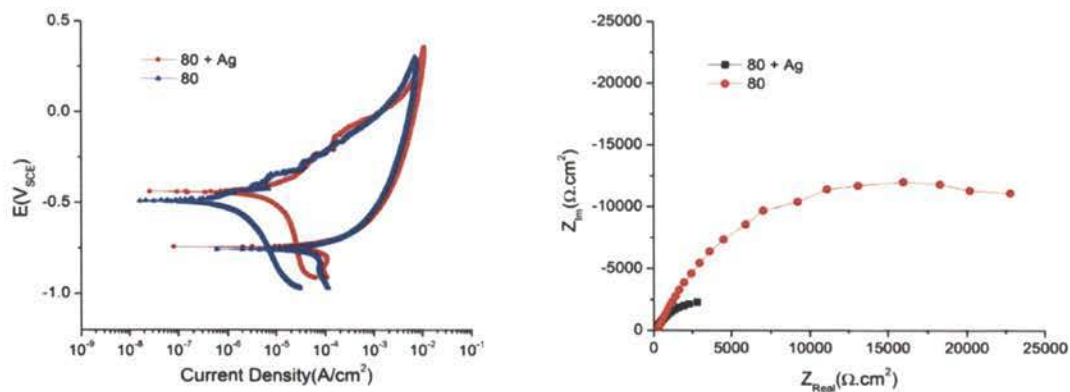
(d)

Figure B1. Potentiodynamic and electrochemical impedance curves for CeCCs electrodeposited with and without silver addition using the pretreatment of 5 minutes in 5wt.% Turco solution at 55°C, and then 5 minutes in 1wt.% Sulfuric acid at a) 50°C, b) 60°C, c) 70°C, d) 80°C.

Potentiodynamic and electrochemical impedance of the CeCCs changed when adding $AgNO_3$ into the $Ce(NO_3)_3$ solution. After activation at 50°C in 1wt.% Sulfuric acid for 5 minutes, adding Ag ion increased the impedance and reduced the corrosion current of the CeCCs. However, at 60°C, 70°C, 80°C, adding Ag ion increased the corrosion current and decreased the impedance is reducing. For the normal CeCCs, the activation temperature was 60°C but with the adding Ag ions, the best activation temperature was 50°C.

Pr AND Ce MIXTURE CONVERSION COATING

(a)

(b)
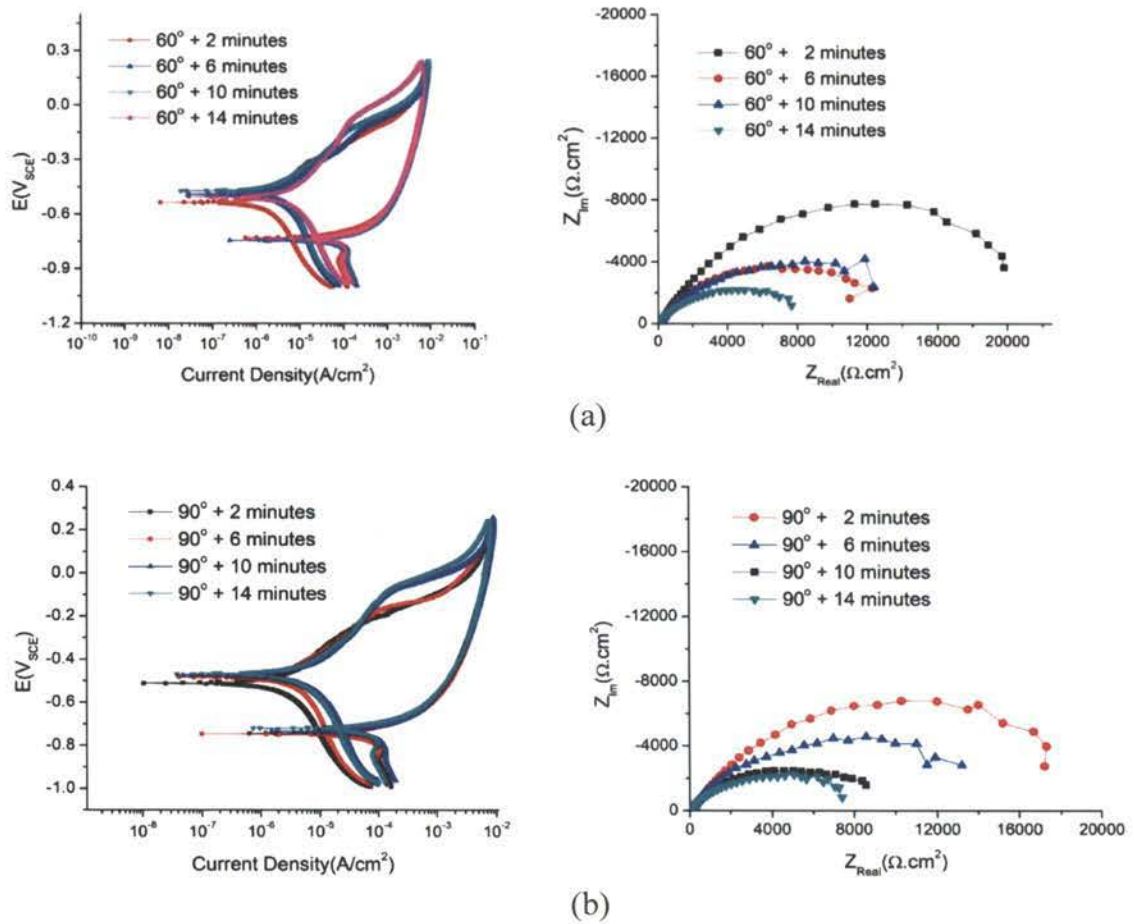
Figure B2. Potentiodynamic and electrochemical impedance of the CeCCs containing Pr deposited on substrate activated in 1wt.% (a) 60°C Sulfuric acid, (b) 90°C Sulfuric acid for 5 minutes.

The corrosion resistance of the CeCCs did not change significantly for different activation temperatures for AA 380, but generally speaking, activation at 60°C in 1wt.% Sulfuric acid was slightly better than 90°C. At both temperatures, the impedance of the CeCCs decreased with increasing immersion time. Correspondingly, the corrosion current increased with increasing immersion time. For activation at 60°C, immersing in the deposition solution for 2 minutes result in coating impedance of 26.3 kΩ•cm2, which is nearly double the impedance produced by immersing in the solution for 6 (13.9

$k\Omega \cdot cm^2$) or 10 minutes (13.7 $k\Omega \cdot cm^2$), also the corrosion current was 0.99 $\mu A/cm2$, half of the corrosion current for 6 (1.87 $\mu A/cm^2$) or 10 minutes (1.90 $\mu A/cm^2$). After 14 minutes of immersion, the impedance decreased to 9.2 $k\Omega \cdot cm^2$ and corrosion current increased to 2.85 $\mu A/cm^2$. For activation at 90°C, the impedance was 21.9 $k\Omega \cdot cm^2$ impedance. After immersion for 2 minutes, which is less than 26.3 $k\Omega \cdot cm^2$, the impedance after 2 minutes for activation at 60°C. For 4 minutes immersion, the impedance decreased to 14.8 $k\Omega \cdot cm^2$, which is similar to13.9 $k\Omega \cdot cm^2$, considering the uncertainty of the measurement. The impedance dropped to 9 $k\Omega \cdot cm^2$ after 10 minutes immersion. The corrosion current increased as the impedance decreased (Table B2).

Table B1. Summary of electrochemical testing for CeCCs deposited on AA 380 for different times for activation temperatures of 60°C or 90°C

Immersion	Corrosion Parameters					
Time	R_p		i_{corr}		E_{corr}	
(min)	($k\Omega \cdot cm^2$)		($\mu A/cm^2$)		(mV_{SCE})	
	60°C	90°C	60°C	90°C	60°C	90°C
2	26.3	21.9	0.99	1.19	-535	-510
6	13.9	14.8	1.87	1.76	-497	-481
10	13.7	8.8	1.90	2.96	-471	-477
14	9.2	8.5	2.85	3.08	-502	-471

VITA

Ci Lin was born on June 26, 1982 in Yong An Fujian China. After graduating from the No.1 High School in Yong An, on July 1, 2002, he pursued an undergraduate degree in material science and engineering from Fuzhou University in Fuzhou, Fujian China, and received his bachelor degree on July 1, 2007. He started to pursue a Master of Science degree in materials science and engineering from the Missouri University of Science and Technology in Rolla, MO at the fall of 2010, which was awarded in May, 2012.